Acta Geochim (2020) 39(5):698–716
https://doi.org/10.1007/s11631-020-00429-z

ORIGINAL ARTICLE

Zircon U–Pb dating, geochemical, and Sr–Nd–Pb–Hf isotopic constraints on the age and origin of intermediate to felsic igneous rocks at South Altyn, Xinjiang, China

Shen Liu[1] · Caixia Feng[1] · Yan Fan[1] · Xiaoqing Chen[2] · Yuhong Yang[1] · Huibo Zhao[1] · Ian M. Coulson[3]

Received: 8 July 2020 / Revised: 5 August 2020 / Accepted: 10 August 2020 / Published online: 26 August 2020

Abstract As a part of a giant trending fault system in the Asian continent and one where a strong zone of left strike-slip fault is present, the Altyn Orogenic belt (AOB) has become an important focus for research. Magmatic rocks are widely distributed across the AOB. However, many investigations have focused primarily on Paleozoic igneous rocks; discussion of Mesozoic related igneous activity is often ignored. Here we present the result of studies of representative diorite and granite rocks outcropping in the AOB, within the Xinjiang Uygur Autonomous Region, South Altyn, China. We present new zircon LA-ICP-MS U–Pb age, geochemical, and Sr–Nd–Pb–Hf isotopic data for these sample suites, identifying them as typical igneous rocks formed between 238 ± 1.5 and 238.8 ± 1.1 Ma. The rocks that we studied fall into the alkaline series, also enriched in light rare earth elements (LREE), some large ion lithophile elements (LILE; e.g., Rb, Ba, Sr, and K), Pb, Th and U, and depleted in heavy rare earth elements (HREE), Nb, Ta, Hf, and Ti. The granite and diorite have high initial $^{87}Sr/^{86}Sr$ ratios (0.7062–0.7114), negative ε_{Nd} (t) values (− 8.8 to − 11.3), ε_{Hf} (t) values (− 8.7 to − 18.7), and relatively constant Pb isotopic ratios (($^{206}Pb/^{204}Pb)_i$ = 6.74–17.884, ($^{207}Pb/^{204}Pb)_i$ = 15.51–15.58, and ($^{208}Pb/^{204}Pb)_i$ = 35.36–38.04), respectively. This suggests that the magmas parental to these rocks were generated from the partial melting of the ancient crust. The parental magmas to these rocks experienced a degree of fractionation of plagioclase, K-feldspar, and hornblende, possibly during rapid magma ascent. Based on these studies, we propose a reasonable model for the origin of the investigated rocks from the Xinjiang Uygur Autonomous Region of South Altyn, which involves crustal thickening, lithospheric extension, and asthenosphere upwelling, that induced crustal melting.

Keywords Altyn orogenic belt · Zircon U–Pb dating · Geochemistry, Sr–Nd–Pb–Hf isotope · Origin

1 Introduction

The Altyn orogenic belt (hereafter AOB) is located at the southwest margin of the Central Asian orogenic belt. It is a complex orogenic belt composed of a series of continental blocks, island arcs, and accretionary units, that extends for ~ 1000 km across China, Russia, Kazakhstan and Mongolia (Li et al. 2020). Moreover, this composite orogenic belt comprises geological units of different geological periods, a variety of structural levels and that formed in distinct tectonic environments. The dominant structures within the AOB are those located in the northern margin of the Qinghai-Tibet Plateau, the southeast margin of the Tarim Basin, the western margin of the Qaidam Basin and the Qilian Kunlun orogenic belt (Luo et al. 2009), whereas the southern part of the belt is limited by the giant Altyn sinistral fault (Wu et al. 2016). From north to south, the AOB can be subdivided into five tectonic units: the North Altyn Block, the North Altyn ophiolitic melange belt, the middle Altyn massif, the South Altyn high pressure and

✉ Shen Liu
liushen@vip.gyig.ac.cn

[1] State Key Laboratory of Continental Dynamics and Department of Geology, Northwest University, 229 Taibai Road, Xi'an 710069, China

[2] College of Earth Sciences, Jilin University, 2199 Jianshe Road, Changchun 130061, China

[3] Solid Earth Studies Laboratory, Department of Geology, University of Regina, Regina, SK S4S 0A2, Canada

ultra-high- pressure (HP–UHP) metamorphic belt, and the Apa-Mangya ophiolite tectonic melange belt (Che and Sun 1996; Wang 1997; Xu et al. 1999; Cui et al. 2002; Liu et al. 2009a, b, 2015; Yang et al. 2012; Wang et al. 2011; Kang et al. 2013; Chen 2018).

The AOB experienced Archean to Paleoproterozoic continental core and crystalline basement formation (Lu and Yuan 2003), plate convergence and collision in the early Neoproterozoic (Qin et al. 2006), plate expansion in the late Neoproterozoic to Early Paleozoic (Liu et al. 1998, 1999), followed by Caledonian plate subduction and collision (Liu et al. 2015; Kang et al. 2016a, b; Wu et al. 2018) and lastly, late Yanshanian large-scale, sinistral faulting (Guo et al. 2008; Wu et al. 2013). As an important part of the northern margin of the Qinghai-Tibet Plateau, the main fault of the southern Altyn Tagh (hereafter South Altyn) forms a principal zone of sinistral faulting in Central Asia. As such, a comprehensive understanding of the formation and evolution history of the South Altyn is of great scientific significance to the division of geological structures in both Northwest China and the Central Asian continent (Wang et al. 2019). For example, this complex tectonic belt owes its formation to the subduction and collision of paleoplates (or blocks) in the Early Paleozoic and experienced a convoluted tectonic evolution process in the Mesozoic (Chen et al. 1995, 1998; Liu et al. 1996; Zhang et al. 1999a, b, 2001a, b, c; Xu et al. 1999; Cui et al. 1999; Ni et al. 2008; Kang et al. 2013; Li et al. 2015). The Early Mesozoic (Triassic) outcrops in this area experience uplift and denudation, while the Middle and Late Mesozoic (Jurassic to Cretaceous) resulted in rifting and a stage of sedimentation (Huang et al. 2004). In recent years, the South Altyn area has become a hot spot for geologists (Zhao et al. 2018). However, the related research has mainly focused on the high-pressure and ultra-high-pressure metamorphism (Liu et al. 1997, 1998, 2002, 2003, 2004, 2005, 2007a, b, c, 2009a, b, c, 2012; Zhang et al. 1999a, 2001a, b, 2002a, b, 2004, 2005; Zhang and Meng 2005; Cao et al. 2009; Wang et al. 2011), ophiolites (Li et al. 2009; Ma et al. 2009), and intermediate felsic intrusive rock (Zhang et al. 1999a, b, 2001a, b, 2002a, b, 2007; Cao et al. 2010; Tian 2009; Sun et al. 2012; Yang et al. 2012; Kang et al. 2013, 2016a, b; Wu et al. 2014, 2016; Liu et al. 2015; Pan et al. 2016; Wang et al. 2019; Li et al. 2020). These studies have provided systematic scientific evidence for the tectonic evolution of the south margin of Altyn Tagh during the Nanhua Early Paleozoic Ocean and transition. Nevertheless, research relating to magmatism and igneous rocks are limited primarily to the Paleozoic period (262–504 Ma); discussion of Mesozoic igneous activity has largely been ignored. Because of this, our paper aims to study and discuss the nature and significance of Mesozoic granite and diorite at Qiemo County, southern margin of the Altyn sinistral Fault Zone. These investigations include zircon U–Pb dating, whole-rock major and trace element compositions, coupled to Sr–Nd–Pb isotope and zircon Hf isotope studies. Based on the above research, a credible genetic age and origin are reasonably determined.

2 Regional geological background and sample petrological characteristics

The protracted evolution of the AOB includes this having experienced ancient Archean crust formation and multi-stage magmatic activities, strong transformation, and intermediate-mafic magmatism during the Paleoproterozoic (2.5–1.8 Ga), Neoproterozoic (1.0–0.8 Ga) collisional orogeny and large-scale magmatism (Wang et al. 2006, 2011; Liu et al. 2009a, b, c), as well as, complex, structural belt formation by subduction and collision of ancient plates (or blocks) in the Early Paleozoic, that were later transformed by a Mesozoic–Cenozoic sinistral fault system. The South Altyn is located between the southern Altyn sinistral Fault and the southern margin fault of Altyn (Liu et al. 1998; Wang et al. 1999), it differs from the Sulu-Dabie ultra-high pressure metamorphic belt which represents an area of deep subduction collision within the Yangtze Craton (Suo et al. 2004).

The present study area is located in the complex rock of the Ananmanya tectonic belt (Fig. 1), mainly comprising old metamorphic rocks (500–1000 Ma; granite and granite gneiss; Liu et al. 2007a, 2015; Lu et al. 2008; Wang et al. 2008; Song et al. 2012; Fan et al. 2019), such as the Paleo-Proterozoic Altyn Group, middle Proterozoic Bashkorgan Group, and the Neoproterozoic Solcuri Group, as well as, Mesozoic-Jurassic, Cenozoic-Paleogene, Neogene and Quaternary systems. Mafic–ultramafic rocks and intermediate-felsic rocks of the Jinning, Caledonian, Hercynian, and Yanshanian periods are very well developed in the study area, and they are distributed in a beaded pattern along the southern edge of the South Altyn, forming relatively large rock units. In addition, intermediate-felsic rocks are mainly distributed in the southern part of the main fault zone.

Samples for this study were collected at outcrop from Chimo County, South Altyn in the Xinjiang Uygur Autonomous Region, China (Fig. 1). The diorite (sample 17A-44-1-10) has a semi-autochthonous medium-fine-grained equigranular structure. Its mineral composition includes plagioclase, K-feldspar, hornblende, biotite, and minor quartz (< 5 %) (Fig. 2). Locally, diorite is commonly observed interlayered with marble ($\sim$ 4.0 m). The sample 17A-44-1 is selected for zircon separation. In contrast, the granite (e.g., porphyritic granite, K-feldspar

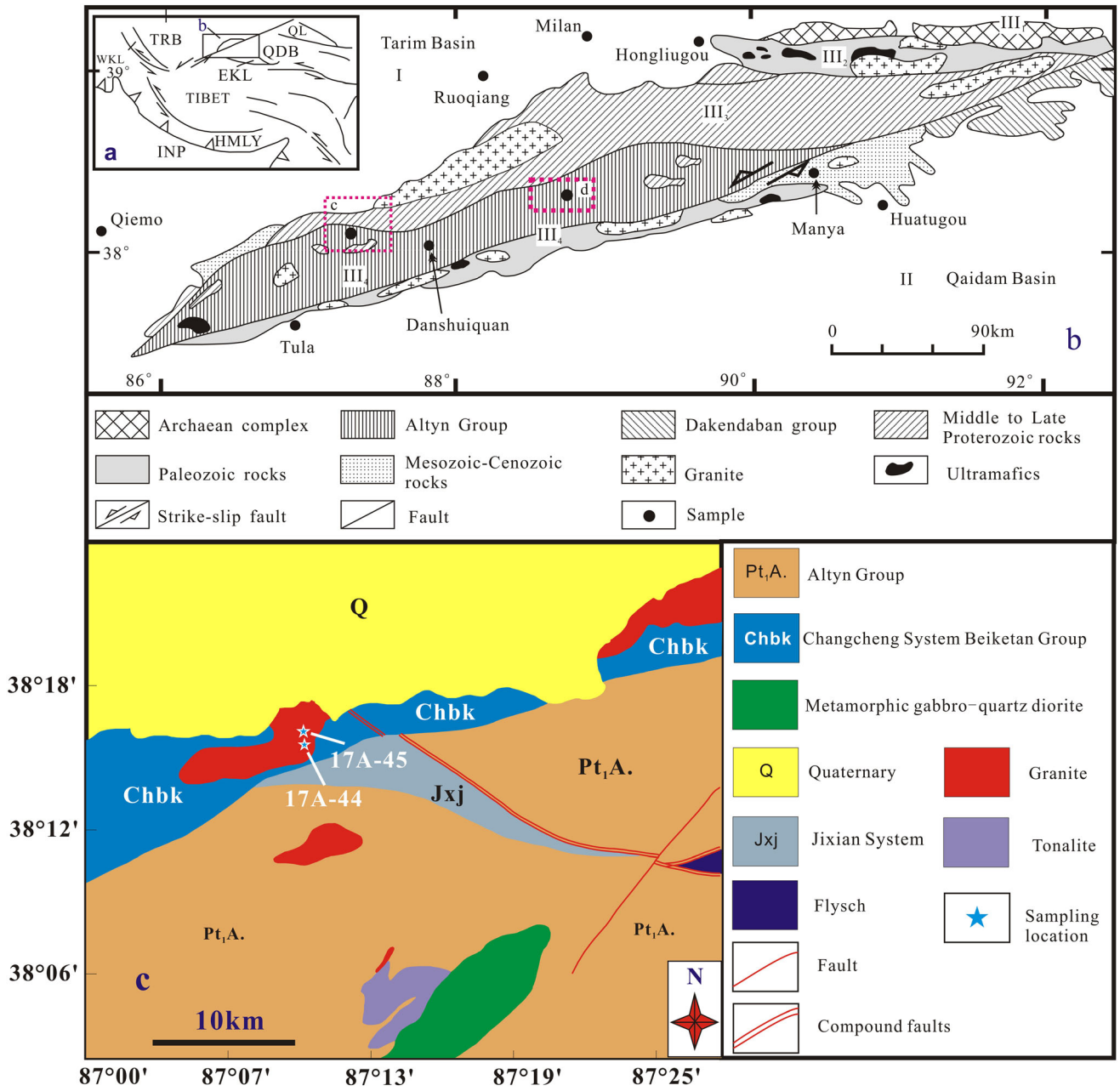

Fig. 1 **a** Tectonic divisions of west China (Liu et al. 2012), **b** geological and tectonic map of the Altyn Tagh Orogen (Liu et al. 2012), and **c** geological map of the southeastern Altyn

granite, and gneissose granite) (sample 17A-45-1-12) has a coarse-grained equigranular structure, and its mineral composition includes semi-autochthonous quartz (45–50 %, 0.2–1.0 cm), autochthonous- semi-autochthonous K-feldspar (35–40 %) and plagioclase (5–10 %) (Fig. 2). Some outcrops of the porphyritic granite have obvious mylonitization and are cut by mafic intrusions (dykes), whereas the gneissose granites have xenoliths within of dark gabbro. Both the dark inclusions and granites have suffered deformation, and each contains tourmaline. And the sample 17A-45-3 is selected for zircon separation.

3 Analytical procedures

3.1 U–Pb dating by laser-ablation-inductively coupled plasma-mass spectrometry (LA-ICP-MS) methods

Zircon from five of the investigated Xinjiang Uygur Autonomous Region samples was separated using conventional heavy liquid and magnetic techniques. Representative zircon grains were then hand-picked under a binocular microscope before being mounted in an epoxy resin disc, polished, and then coated with gold, before the analysis. Individual crystals were studied using optical microscopy techniques and under cathodoluminescence (CL) to aid in characterization and to reveal any internal features. CL imaging (Fig. 2) and the U–Pb analyses were undertaken by LA-ICP-MS methods at the State Key Laboratory of Continental Dynamics, Xi'an, China. The analytical procedures used were those as described in detail in Harris et al. (2004); a spot diameter of 29 μm was used. U–Th–Pb ratios and absolute abundances were determined by reference to replicate measurements of a standard TEMORA zircon and the NIST 610 glass standard (Figs. 3, 4).

3.2 Major elemental and trace elemental analyses

Whole-rock major element compositions were determined using analytical Axioms-advanced X-ray fluorescence (XRF) spectrometer at the State Key Laboratory of Ore Deposit Geochemistry (SKLODG), Guiyang, China with an analytical precision of better than 5 %. Trace element compositions were determined by Inductively-coupled plasma mass-spectrometry (ICP-MS) utilizing a Perkin-Elmer ELAN DRC-e instrument at the SKLODG. Prior to analysis, powdered samples (50 mg) were dissolved in high-pressure Teflon bombs, using an HF + HNO_3 acid attack for 48 h, at a temperature of ~ 190 °C (Qi et al. 2000). Signal drift was monitored during the analysis by reference to an Rh internal standard. GBPG-1, OU-6, GSR-1, and GSR-3 standards were additionally used for analytical quality control with a determined analytical precision of better than 5 %.

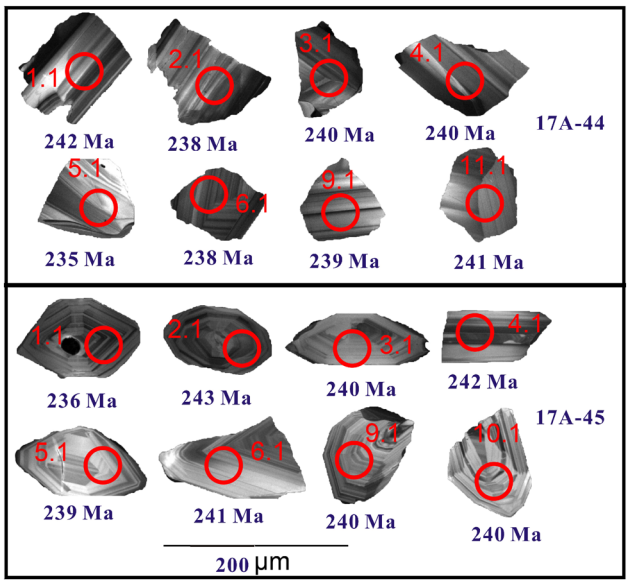

Fig. 2 Representative cathodoluminescence (CL) images for zircon in the rocks from the Xinjiang Uygur Autonomous Region of South Altyn

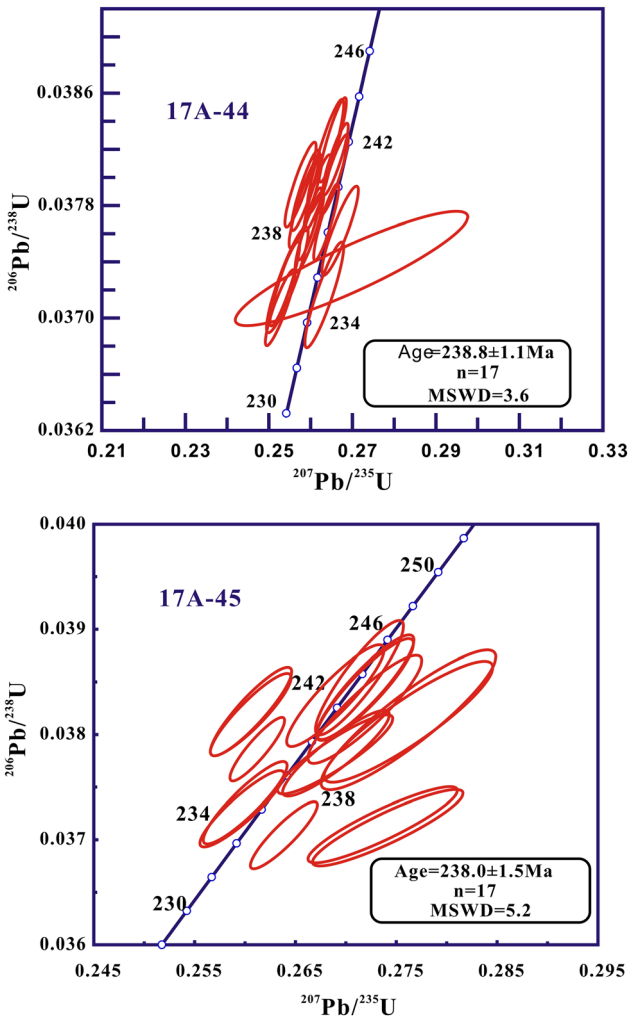

Fig. 3 The corresponding LA-ICP-MS U–Pb concordia diagrams for the rocks studied from the Xinjiang Uygur Autonomous Region of South Altyn

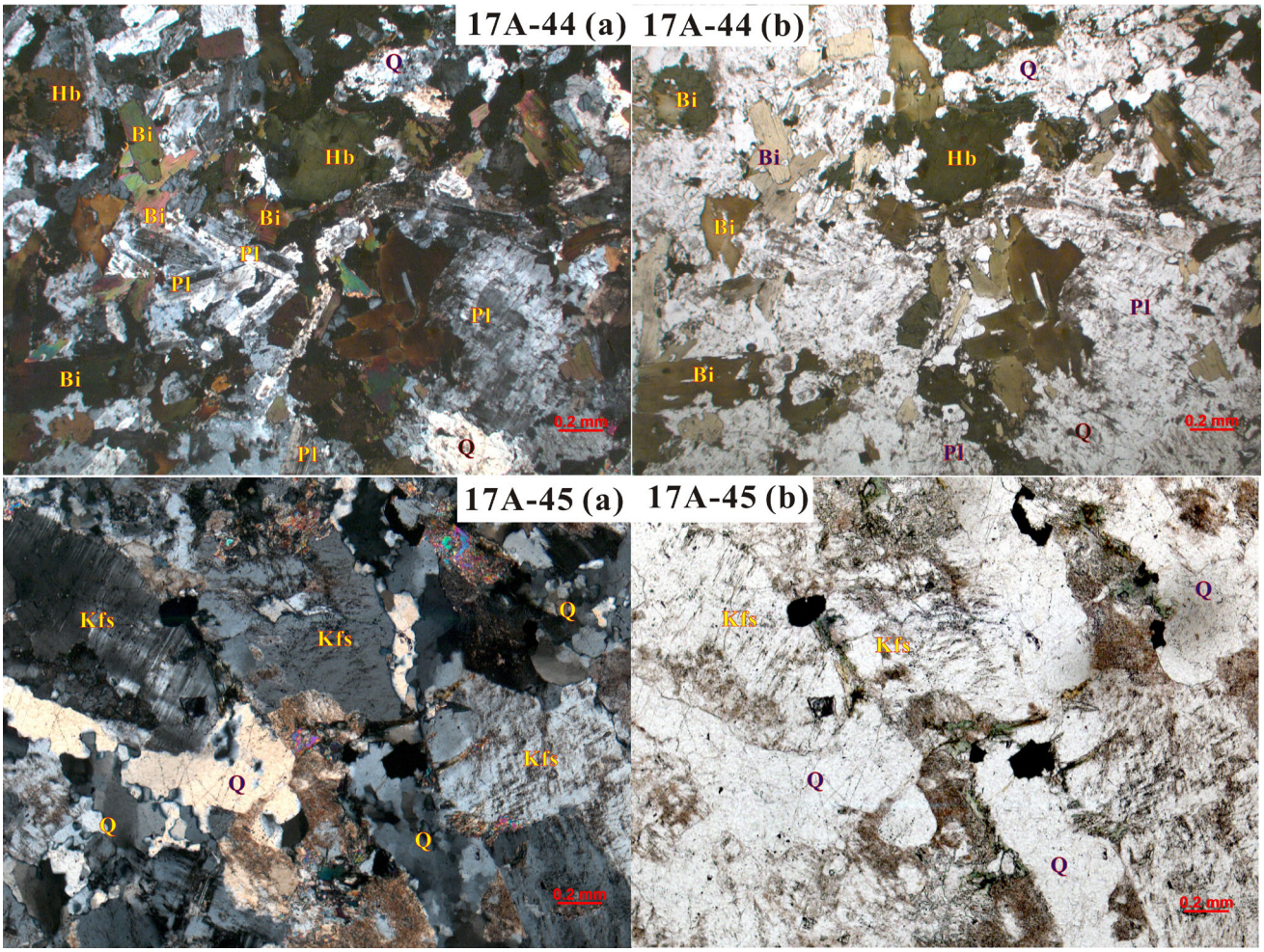

Fig. 4 Representative photomicrographs of the studied granitic rock from the Xinjiang Uygur Autonomous Region of South Altyn. Key: Q: quartz, Pl: plagioclase, Bi: biotite, Hb: hornblende, Kfs: K-feldspar

3.3 Sr–Nd–Pb isotopic analyses

For Rb–Sr and Sm–Nd isotope analyses, sample powders were spiked with mixed isotope tracers, following dissolution with HF + HNO_3 acids (in Teflon bombs). The isotopes were separated by conventional cation-exchange techniques. Isotopic measurements were performed using a Finnigan Triton Ti thermal ionization mass spectrometer (TIMS) at the SKLODG. Procedural blanks yielded concentrations of < 200 pg for Sm and Nd, and < 500 pg for Rb and Sr, respectively. The mass fractionation corrections for Sr and Nd isotopic ratios were based on $^{86}Sr/^{88}Sr = 0.1194$ and $^{146}Nd/^{144}Nd = 0.7219$. Analysis of the NBS987 and La Jolla standards yielded the following results: $^{87}Sr/^{86}Sr = 0.710246 \pm 16$ (2σ), and $^{143}Nd/^{144}Nd = 0.511863 \pm 8$ (2σ), respectively. Prior to Pb isotopic analysis, Pb was separated and purified by conventional cation-exchange techniques, using diluted HBr as an eluent. Analysis of the NBS981 standard yielded mean values for $^{204}Pb/^{206}Pb$ of 0.0896 ± 15, $^{207}Pb/^{206}Pb$ of 0.9145 ± 8, and $^{208}Pb/^{206}Pb$ of 2.162 ± 2.

3.4 In-situ zircon Hf isotopic analysis

In-situ zircon Hf isotopic analyses were conducted using a Neptune multi-collector system (MC-ICP-MS), equipped with a 193 nm laser, at the Institute of Geology and Geophysics, Chinese Academy of Sciences in Beijing, China. During the analysis, a laser repetition rate of 10 Hz at 100 mJ was used with spot sizes of 32 and 63 μm. Raw count rates for ^{172}Yb, ^{173}Yb, ^{175}Lu, $^{176}(Hf + Yb + Lu)$, ^{177}Hf, ^{178}Hf, ^{179}Hf, ^{180}Hf, and ^{182}W were collected and isobaric interference corrections for ^{176}Lu and ^{176}Yb on ^{176}Hf were determined precisely.^{176}Lu was calibrated using the ^{175}Lu value and a correction was made to ^{176}Hf. The $^{176}Yb/^{172}Yb$ value of 0.5887 and mean β_{Yb} value obtained

during Hf analysis on the same spot were applied for the interference correction of ^{176}Yb on ^{176}Hf (Iizuka and Hirata 2005). Details of the analytical techniques employed are described in Xu et al. (2004) and Wu et al. (2006). During the analysis, the determined ^{176}Hf/^{177}Hf and ^{176}Lu/^{177}Hf ratios of the standard zircon (91500) were 0.282300 ± 15 (2σn, n = 24) and 0.00030, respectively, which are similar to the commonly accepted ^{176}Hf/^{177}Hf ratio of 0.282302 ± 8 and 0.282306 ± 8 (2σ) measured using the solution method (Goolaerts et al. 2004; Woodhead et al. 2004).

4 Results

4.1 Zircon U–Pb dating

Clean, prismatic grains of euhedral zircon in samples 17A-44 and 17A-45 series display evident oscillatory zoning, suggesting that these were the products of a crystallizing magma. A total of 17 zircon grains provided a weighted mean ^{206}Pb/^{238}U age of 238.8 ± 1.1 Ma (1σ) (95 % confidence interval, MSWD = 3.6) for 17A-44 (Table 1), whereas 17 zircon grains from sample 17A-45 gave a weighted mean ^{206}Pb/^{238}U age of 238.0 ± 1.5 Ma (1σ) (95 % confidence interval, MSWD = 5.2) (Table 1). These determinations are the best estimates for the crystallization ages of the investigated intermediate and felsic intrusive rocks from the Xinjiang Uygur Autonomous Region. No inherited zircon characteristics were observed in the investigated sample populations.

4.2 Major and trace elements

Whole-rock geochemical data for the studied rocks are presented in Tables 2 and 3. The diorite samples exhibit a fairly narrow range of compositions (Table 2); each is situated within the alkaline field in terms of the total alkali-silica diagram (Fig. 5). By contrast, the granite samples exhibit a relatively wide range of compositions (Table 2). While all of the granite samples also fall into the alkaline field in terms of the total alkali-silica diagram (Fig. 5a), they additionally reside within the shoshonitic series field in terms of a plot of Na_2O versus K_2O (Fig. 5b) and are metaluminous (A/CNK = 0.7–1.0; Fig. 5c) in terms of aluminum saturation (Maniar and Piccoli 1989; Ji et al. 2016). Moreover, all samples studied are characterized by light rare earth element (LREE) enrichment and heavy rare earth element (HREE) depletion, with a narrow range of Eu/Eu* (0.73–1.05) and high $(La/Yb)_N$ ratios (61–169) (Table 3 and Fig. 6a, b). On primitive mantle-normalized trace element diagrams, the studied rocks show enrichment in LILEs (i.e., Rb, Ba, Sr, K), Th, U and Pb, and depletion for HFSEs (i.e., Nb, Ta, Hf, and Ti) (Fig. 6b).

4.3 Sr–Nd–Pb isotopes

Sr, Nd, and Pb isotopic data for 14 representative rocks from this study are presented in Tables 4, 5 and Figs. 7, 8a, b. The diorite samples exhibit a wide range in $(^{87}Sr/^{86}Sr)_i$ values of between 0.7062 to 0.7090 and wide variation in ε_{Nd} (t) values, from − 9.1 to − 11.3. The granite samples similarly exhibit a wide range in $(^{87}Sr/^{86}Sr)_i$ values of between 0.705 to 0.7114 and wide variation in ε_{Nd} (t) values, from − 8.8 to − 10.5. These data are suggestive of source areas with slight enrichment. The investigated diorite rocks display relatively constant Pb isotopic ratios of: $(^{206}Pb/^{204}Pb)_i$ = 16.61–17.88, $(^{207}Pb/^{204}Pb)_i$ = 15.56–15.58 and $(^{208}Pb/^{204}Pb)_i$ = 37.47–38.04. The investigated granite units also display relatively constant Pb isotopic ratios of: $(^{206}Pb/^{204}Pb)_i$ = 17.03–17.76, $(^{207}Pb/^{204}Pb)_i$ = 15.45–15.55 and $(^{208}Pb/^{204}Pb)_i$ = 37.10–37.69.

4.4 Zircon Hf isotope analysis

The results for zircon Hf isotope analyses in the studied samples are listed in Table 6. Twenty-five spot analyses were obtained for sample 17A-44, yielding very uniform ε_{Hf} (t) values of between −8.7 and −11.2, which correspond to T_{DM2} model ages of between 1814 and 1976 Ma (Figs. 9, 10). Twenty-five spot analyses were obtained for sample 17A-45; they show a lower range of ε_{Hf} (t) values of between −14.5 and −18.7, corresponding to T_{DM2} model ages of between 2182 and 2440 Ma (Figs. 9, 10).

5 Discussion

As one of the most widely distributed rock types and an important sign of continental crustal growth, intermediate-felsic igneous rock, especially granite, is an excellent window and research object in studies of the growth and tectonism of continental crust (Xiao et al. 2005). For example, based upon the study of granites in the Lachlan fold belt of Australia, the classification of the S-type, I-type, A-type, and M-type granites were proposed (Chappell and White 1974; White and Chappell 1983). A-type is used to describe felsic rocks, which in addition to appearing in anorogenic tectonic settings, are more alkaline. A-type granites appear to be polygenetic, with no single process accounting for them all. Such magmas can form through melting of the lower crust under conditions that are usually extremely dry, or in the fractionation of basaltic magma. M-type covers those granites that derive

Table 1 LA-ICP-MS U–Pb isotopic data for zircon from the studied rocks of Xinjiang Uygur Autonomous Region of South Altyn

Spot	Th (ppm)	U (ppm)	Pb (ppm)	Th/U	$^{207}Pb/^{206}Pb$	1s	$^{207}Pb/^{235}U$	1s	$^{206}Pb/^{238}U$	1s	$^{207}Pb/^{206}Pb$	1s	$^{207}Pb/^{235}U$	1s	$^{206}Pb/^{238}U$	1s
17A-44	*Isotopic ratios*											*Age (Ma)*				
17A-44-01	134	542	393	1.38	0.0503	0.0003	0.2654	0.0022	0.0383	0.0002	207	10	239	2	242	1
17A-44-02	159	641	565	1.14	0.0500	0.0003	0.2598	0.0019	0.0377	0.0002	195	9	235	2	238	1
17A-44-03	109	433	431	1.01	0.0495	0.0003	0.2588	0.0022	0.0379	0.0002	170	11	234	2	240	1
17A-44-04	154	622	535	1.16	0.0501	0.0003	0.2617	0.0021	0.0379	0.0002	198	10	236	2	240	1
17A-44-05	132	549	337	1.63	0.0494	0.0004	0.2528	0.0023	0.0371	0.0002	169	13	229	2	235	1
17A-44-06	261	1052	573	1.83	0.0501	0.0004	0.2597	0.0023	0.0376	0.0002	198	11	234	2	238	1
17A-44-07	239	995	484	2.06	0.0494	0.0004	0.2538	0.0024	0.0372	0.0002	168	12	230	2	236	1
17A-44-08	60.2	242	194	1.25	0.0495	0.0005	0.2544	0.0033	0.0373	0.0003	169	18	230	3	236	2
17A-44-09	56.5	226	147	1.53	0.0496	0.0005	0.2588	0.0026	0.0378	0.0002	177	13	234	2	239	1
17A-44-10	123	508	301	1.69	0.0492	0.0004	0.2576	0.0024	0.0380	0.0002	157	13	233	2	240	1
17A-44-11	181	711	485	1.47	0.0507	0.0004	0.2657	0.0022	0.0380	0.0002	225	10	239	2	241	1
17A-44-12	137	557	293	1.90	0.0501	0.0005	0.2636	0.0029	0.0382	0.0003	199	13	238	2	241	2
17A-44-13	69.7	215	189	1.14	0.0524	0.0036	0.2698	0.0184	0.0374	0.0003	302	143	243	15	236	2
17A-44-14	33.2	85	657	0.13	0.0507	0.0003	0.2638	0.0020	0.0377	0.0002	228	9	238	2	238	1
17A-44-15	348	1420	629	2.26	0.0507	0.0003	0.2660	0.0020	0.0381	0.0002	228	10	239	2	241	1
17A-44-16	75.9	310	184	1.68	0.0515	0.0005	0.2671	0.0029	0.0376	0.0002	261	15	240	2	238	1
17A-44-17	69.7	289	176	1.64	0.0514	0.0005	0.2633	0.0031	0.0372	0.0003	258	15	237	2	235	2
17A-45	*Isotopic ratios*											*Age (Ma)*				
17A-45-01	43.4	178	151	1.18	0.0512	0.0003	0.2719	0.0032	0.0384	0.0003	224	14	235	2	236	1
17A-45-02	130	560	549	1.02	0.0512	0.0003	0.2719	0.0032	0.0385	0.0003	249	13	244	3	243	2
17A-45-03	41.7	169	143	1.19	0.0512	0.0003	0.2690	0.0032	0.0384	0.0003	179	14	235	2	240	1
17A-45-04	39.0	161	162	1.00	0.0515	0.0005	0.2719	0.0037	0.0382	0.0003	263	16	244	3	242	2
17A-45-05	43.2	182	124	1.47	0.0523	0.0006	0.2762	0.0055	0.0381	0.0004	165	19	233	3	239	2
17A-45-06	52.3	214	170	1.26	0.0522	0.0007	0.2762	0.0057	0.0381	0.0004	296	27	248	5	241	3
17A-45-07	56.7	230	222	1.04	0.0495	0.0004	0.2606	0.0026	0.0382	0.0003	170	12	235	2	242	2
17A-45-08	34.6	145	123	1.18	0.0495	0.0004	0.2606	0.0027	0.0382	0.0003	133	16	227	2	236	1
17A-45-09	39.7	160	152	1.05	0.0535	0.0008	0.2736	0.0049	0.0371	0.0002	186	12	235	2	240	1
17A-45-10	49.4	208	160	1.30	0.0534	0.0008	0.2741	0.0049	0.0371	0.0002	347	29	246	4	235	2
17A-45-11	222	924	916	1.01	0.0500	0.0003	0.2612	0.0018	0.0379	0.0002	196	7	236	1	240	1
17A-45-12	150	625	613	1.02	0.0505	0.0005	0.2597	0.0028	0.0373	0.0002	180	8	234	2	240	1
17A-45-13	48.9	203	190	1.07	0.0505	0.0005	0.2600	0.0027	0.0374	0.0003	217	12	235	2	236	2
17A-45-14	111	467	465	1.00	0.0516	0.0004	0.2638	0.0022	0.0370	0.0002	269	10	238	2	234	1
17A-45-15	59.8	246	265	0.93	0.0515	0.0004	0.2689	0.0038	0.0378	0.0003	235	10	234	2	234	1
17A-45-16	98.7	379	514	0.74	0.0510	0.0003	0.2713	0.0029	0.0385	0.0004	242	11	244	2	244	2
17A-45-17	78.6	328	309	1.06	0.0515	0.0004	0.2690	0.0035	0.0378	0.0003	262	17	242	3	239	2

Table 2 Major oxides (wt %) of the studied rocks from Xinjiang Uygur Autonomous Region of South Altyn

Sample	Rock-type	SiO_2	TiO_2	Al_2O_3	Fe_2O_3	MnO	MgO	CaO	Na_2O	K_2O	P_2O_5	LOI	Total	$Mg^{\#}$	T (°C)
17A-44-1	Diorite	50.27	0.98	18.36	9.76	0.09	3.68	5.81	4.43	3.78	1.02	0.95	99.15	45.4	754
17A-44-2	Diorite	52.35	0.86	20.94	6.32	0.08	2.10	5.15	5.27	2.93	0.59	2.54	99.13	42.2	759
17A-44-3	Diorite	51.83	0.95	18.40	8.56	0.13	3.01	5.61	4.30	3.16	1.04	2.22	99.20	43.6	845
17A-44-4	Diorite	52.14	1.02	19.62	6.73	1.02	2.13	5.23	5.32	3.15	0.61	2.33	99.30	41.1	899
17A-44-5	Diorite	52.16	0.95	19.58	6.81	0.82	2.36	5.25	5.41	3.22	0.55	2.14	99.25	43.3	771
17A-44-6	Diorite	51.85	0.93	18.64	8.42	0.12	2.95	5.36	4.34	3.19	1.02	2.35	99.17	43.5	754
17A-44-7	Diorite	51.93	0.85	18.72	8.24	0.11	2.84	5.43	4.36	3.24	0.96	2.45	99.13	43.1	849
17A-44-8	Diorite	52.15	0.98	19.61	6.65	0.91	2.24	5.32	5.34	3.16	0.57	2.41	99.34	42.6	899
17A-44-9	Diorite	52.42	0.83	21.05	6.28	0.06	1.93	5.04	5.32	2.95	0.56	2.83	99.27	40.3	863
17A-44-10	Diorite	50.33	0.95	18.42	9.62	0.07	3.45	5.78	4.45	3.82	0.94	1.35	99.18	44.1	889
17A-45-1	Granite	72.34	0.21	14.55	0.94	0.01	0.31	1.11	4.08	5.38	0.05	0.92	99.89	42.2	835
17A-45-2	Granite	72.70	0.12	14.55	0.56	0.01	0.19	0.99	4.29	5.27	0.03	1.00	99.71	42.8	787
17A-45-4	Granite	73.01	0.02	14.67	0.28	0.01	0.05	0.79	5.15	5.10	0.01	0.79	99.88	29.4	731
17A-45-5	Granite	65.67	0.36	15.58	2.45	0.07	0.75	2.38	4.33	7.44	0.11	0.62	99.73	40.1	905
17A-45-6	Granite	65.73	0.33	15.63	2.32	0.05	0.73	2.36	4.35	7.46	0.09	0.39	99.44	40.9	904
17A-45-8	Granite	66.14	0.28	15.65	2.23	0.05	0.74	2.35	4.34	7.45	0.08	0.35	99.66	42.2	909
17A-45-9	Granite	72.36	0.19	14.58	0.92	0.01	0.27	0.96	4.12	5.38	0.04	0.76	99.59	39.2	834
17A-45-11	Granite	72.65	0.13	14.53	0.58	0.03	0.22	1.02	4.24	5.25	0.05	0.92	99.62	45.5	797
17A-45-12	Granite	72.96	0.03	14.58	0.32	0.03	0.06	0.81	5.13	5.03	0.03	0.76	99.74	29.2	805

from mafic or intermediate magmas, generally sourced from the mantle. These are rare, usually occurring only in oceanic crust within an ophiolite suite, and mostly associated with basalt and meta aluminous plagioclase granite. In general, the aluminous saturation index (A/CNK; Maniar and Piccoli 1989) is used to delineate the boundary between I-type (igneous protolith) granite and S-type (sedimentary protolith) granite. Rocks with an A/CNK of > 1.1 are strongly peraluminous, and typically belong to the S-type granite; a value for A/CNK of < 1.1 is weakly aluminous and representative of I-type granite.

5.1 The source of the Xinjiang Uygur Autonomous Region magmas

The rocks investigated from Xinjiang Uygur Autonomous Region are characterized by the following isotopic compositions: high $(^{87}Sr/^{86}Sr)_i$ = (0.7062–0.7114), $(^{206}Pb/^{204}Pb)_i$ = (16.74–17.88), $(^{207}Pb/^{204}Pb)_i$ = (15.51–15.58), and $(^{208}Pb/^{204}Pb)_i$ = (35.36–38.04), negative ε_{Nd} (t) and ε_{Hf} (t) values of (− 8.8 to − 11.3, and −8.7 to −11.2), and high $(La/Yb)_N$ ratios of 61–169 (see Table 3, 4, 5, 6; Figs. 6a, b, 7, 8a, b, 9, 10), implying that they were derived from a relatively enriched magma source area. In addition, the diorite and granite samples have negative ε_{Hf} (t) (− 8.7 to − 11.2, and − 14.5 to − 18.7) relating to an older two-stage model age (1.8–2.0 Ga, 2.2–2.4 Ga), which indicates that the rocks likely derived from an ancient crustal source (Taylor and McClennan 1985; Wu et al. 2007). This is further supported by their higher SiO_2 contents (50.27–72.96, Table 2). Although the rocks studied have similar REE, trace element and isotopic characteristics, there are also some important differences. Such characteristics indicate that the granite and diorite investigated from Xinjiang Uygur Autonomous Region may have two different sources or origins.

To decipher if and how mantle materials may have participated in the genetic process of these rocks requires some explanation. In general, there are two ways for mantle material to influence a source area: 1. The mantle-derived components can provide heat input to induce partial melting of crustal materials and thereby produce a spectrum of magma compositions, depending upon the heterogeneity of source materials. As such, felsic magma may directly be linked at its source to the formation of diorite (Griffin et al. 2002; Kemp et al. 2007; Zhao et al. 2010, 2012). 2. The lower crust was formed through the underplating of mantle-derived components, and then partially melted to form diorite under the influence of later thermal events (Jahn et al. 2000; Wu et al. 2006; Zheng et al. 2007). Generally, the two-stage model ages of igneous rocks are quite different from their metamorphic

Table 3 The trace elements analysis results (ppm) for the studied rocks from Xinjiang Uygur Autonomous Region of South Altyn

Sample	Sc	V	Cr	Ni	Rb	Sr	Y	Zr	Nb	Ba	La	Ce	Pr	Nd	Sm	Eu
17A-44-1	6.67	159	11.8	6.55	83.4	4730	19.2	112	7.57	8050	223	473	55.1	209	27.9	6.42
17A-44-2	5.66	79.9	80.3	26.2	78.1	825	11.3	95.1	5.72	4850	70.3	139	16.8	65.8	15.1	4.23
17A-44-3	15.6	149	35.1	38.7	172	3620	52.1	282	8.23	9180	331	765	92.0	352	51.8	11.4
17A-44-4	17.8	155	38.9	41.5	233	4010	59.2	465	10.1	8960	694	1310	142	464	60.7	12.9
17A-44-5	6.72	176	12.2	7.81	85.3	3215	21.3	123	7.64	7864	235	482	55.3	212	28.3	6.44
17A-44-6	5.78	82.3	91.5	28.4	81.4	763	12.4	98.4	5.82	4936	71.4	146	17.3	66.2	14.3	4.25
17A-44-7	15.8	153	35.4	39.5	175	3851	52.4	285	8.14	8940	342	772	92.3	356	52.4	11.6
17A-44-8	17.6	158	39.3	41.8	242	3935	60.4	473	10.4	8855	708	1262	145	471	61.2	13.3
17A-44-9	16.4	162	35.6	40.6	183	3462	52.6	295	8.32	8815	352	786	93.4	368	52.6	12.2
17A-44-10	18.1	165	40.2	42.3	245	3528	60.6	482	10.3	8685	723	1355	153	484	62.3	13.5
17A-45-1	1.38	6.87	2.05	0.77	158	532	5.40	170	5.59	5266	243	481	56.3	213	32.30	6.45
17A-45-2	0.62	4.89	4.84	1.16	158	398	6.86	99.5	7.14	5358	72.4	144	17.3	66.4	15.40	4.25
17A-45-4	0.16	2.52	2.12	0.76	167	331	14.50	52.3	5.44	5359	344	768	94	361	53.50	12.30
17A-45-5	1.43	27.6	3.79	1.63	198	696	27.2	443	10.2	5391	703	1322	146	472	62.2	13.3
17A-45-6	1.36	27.2	3.66	1.58	194	682	26.5	437	9.65	5286	246	486	57.2	224	36.5	6.54
17A-45-8	1.45	27.8	3.82	1.65	205	703	27.4	452	10.4	5342	72.6	152	18.3	68.1	14.6	4.28
17A-45-9	1.43	6.85	2.03	0.75	156	535	5.43	166	5.62	5329	352	775	94.2	363	53.4	12.3
17A-45-11	0.65	4.93	4.86	1.15	162	406	6.73	112	7.16	5399	716	1272	154	474	62.3	14.2
17A-45-12	0.72	5.14	4.92	1.16	175	413	6.76	127	7.25	5376	358	794	94.5	375	54.5	13.4

Sample	Gd	Tb	Dy	Ho	Er	Tm	Yb	Lu	Hf	Ta	Pb	Th	U	Eu/Eu*	$(La/Yb)_N$
17A-44-1	13.2	1.27	4.55	0.62	1.34	0.16	0.99	0.14	2.70	0.30	45.3	46.6	12.8	0.90	152
17A-44-2	8.39	0.93	2.68	0.38	0.91	0.12	0.78	0.11	2.16	0.30	47.6	52.4	13.1	1.05	61
17A-44-3	28.3	3.01	11.7	1.73	3.78	0.47	2.78	0.39	6.62	0.28	67.2	64.5	13.6	0.83	80
17A-44-4	31.9	3.38	12.9	1.88	4.12	0.50	2.95	0.41	8.14	0.36	97.7	77.4	10.5	0.81	159
17A-44-5	13.5	1.28	4.57	0.63	1.36	0.15	0.98	0.15	2.72	0.31	45.5	48.5	11.8	0.89	162
17A-44-6	9.41	0.82	2.83	0.39	0.93	0.13	0.79	0.13	2.15	0.32	48.2	54.3	13.3	1.05	61
17A-44-7	28.5	3.04	11.8	1.75	3.82	0.48	2.83	0.42	6.64	0.32	67.4	65.3	13.5	0.83	81
17A-44-8	32.3	3.42	13.2	1.86	4.14	0.52	2.96	0.43	8.15	0.36	98.2	77.6	10.7	0.83	161
17A-44-9	29.1	3.06	12.3	1.83	3.85	0.51	2.85	0.43	6.65	0.34	68.2	67.2	14.1	0.87	83
17A-44-10	32.6	3.45	13.6	1.91	4.16	0.54	2.98	0.45	8.18	0.38	98.4	78.1	15.1	0.82	164
17A-45-1	13.5	1.32	4.63	0.63	1.36	0.15	0.99	0.14	0.83	0.39	37.7	83.2	15.1	0.81	165
17A-45-2	8.44	0.95	2.74	0.43	0.94	0.13	0.78	0.11	0.92	0.43	37.6	80.5	14.5	1.04	62
17A-45-4	29.40	3.06	12.40	1.81	3.81	0.48	2.78	0.39	1.61	0.52	32.9	65.6	13.2	0.86	83
17A-45-5	33.1	3.45	13.40	1.94	4.16	0.54	2.95	0.41	1.52	0.45	34.0	76.2	14.0	0.81	161
17A-45-6	14.3	1.35	4.64	0.65	1.38	0.16	0.98	0.15	1.54	0.43	33.7	75.8	13.8	0.73	169
17A-45-8	9.44	0.84	2.85	0.42	0.95	0.14	0.79	0.13	1.52	0.43	33.9	76.4	14.2	1.05	62
17A-45-9	29.2	3.06	12.40	1.82	3.91	0.52	2.83	0.42	1.51	0.38	37.5	82.3	14.60	0.87	84
17A-45-11	33.5	3.46	13.40	1.93	4.16	0.54	2.96	0.43	1.53	0.44	37.5	84.5	14.70	0.86	163
17A-45-12	31.2	3.13	13.10	1.91	3.42	0.53	2.85	0.43	1.52	0.43	37.6	83.6	14.50	0.91	85

ages; the possibility of the second mode of genesis thus is plausibly ruled out in this study.

5.2 Fractional crystallization

On Harker plots (Fig. 11), with increasing SiO_2 content, MgO, TiO_2, and Fe_2O_3 decrease, which shows a typical

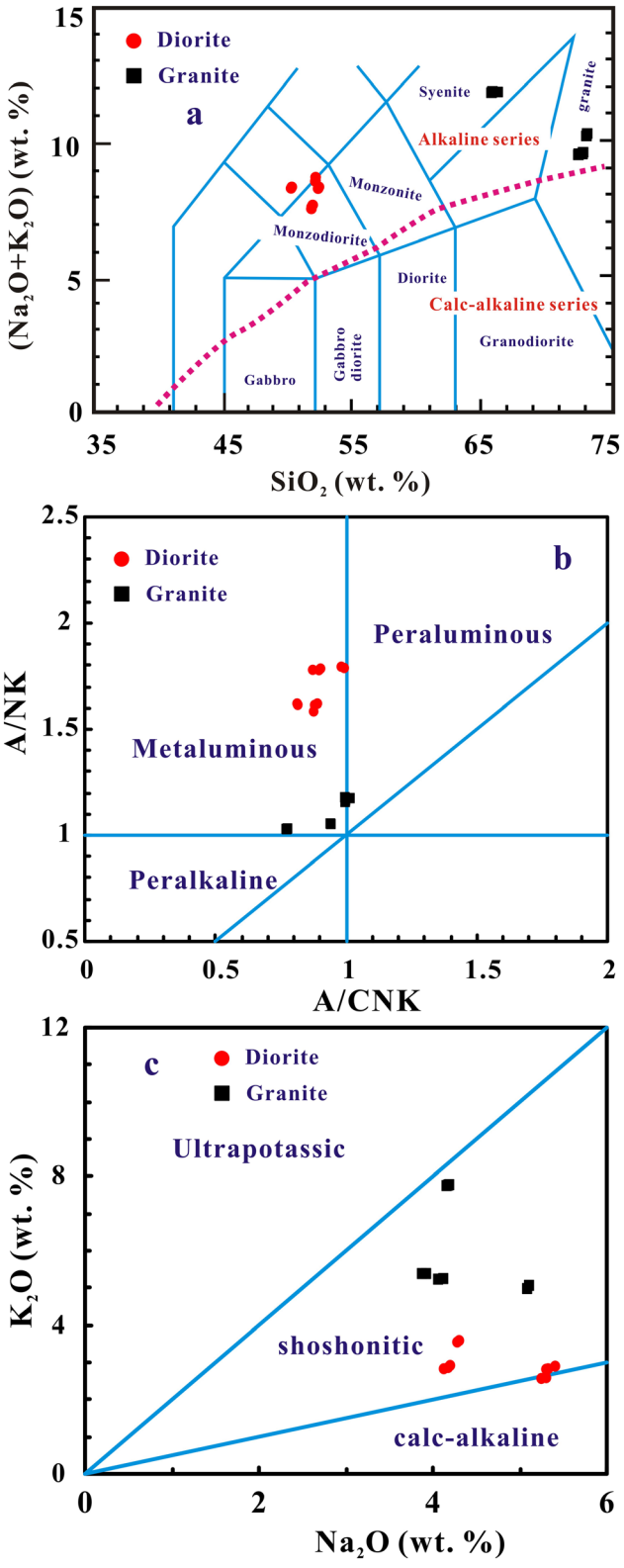

◀**Fig. 5** Classification of the granitic rocks from the Xinjiang Uygur Autonomous Region on the basis of: **a** the total-alkali versus SiO_2 (TAS) diagram. All the major element data have been recalculated to 100 % on a LOI-free basis (Middlemost 1994; Le Maitre 2002); **b** K_2O versus Na_2O diagram, showing the alkaline association to be shoshonitic (Middlemost 1972); and (c) $Al_2O_3/(Na_2O + K_2O)$ molar versus $Al_2O_3/(CaO + Na_2O + K_2O)$ molar plot (Maniar and Piccoli 1989)

magmatic mixing or fractional crystallization (e.g., K-feldspar and hornblende) evolutionary trend. Moreover, Na_2O does not change greatly with an increase of SiO_2, but Al_2O_3 and CaO decrease as SiO_2 increases. The negative anomalies observed for Eu and Sr in the investigated rocks (Table 3, Fig. 6a, b) indicate that plagioclase crystallization was important during magma evolution. However, the fractional crystallization of plagioclase in granite is relatively weaker than for diorite, reflecting its lower Sr contents (Table 3, Fig. 6a, b).

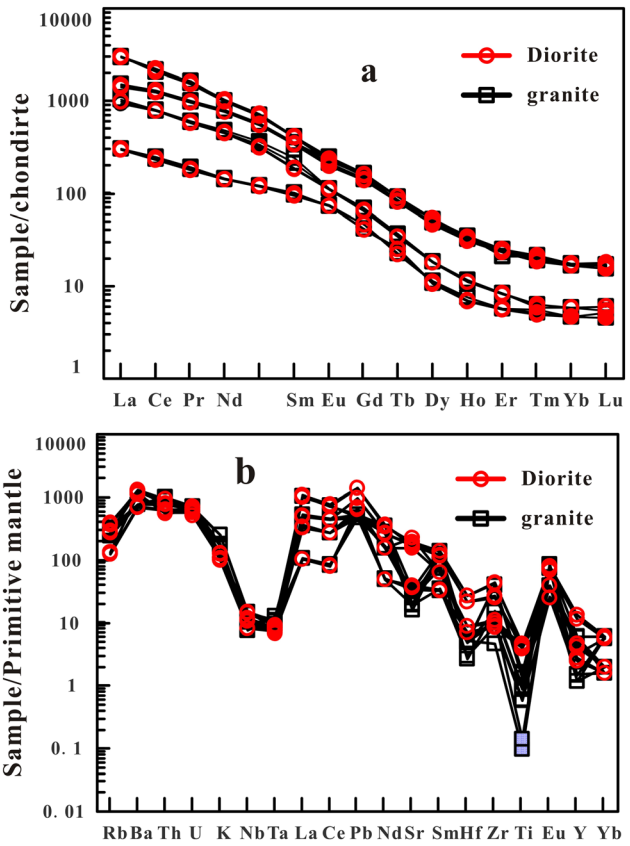

Fig. 6 **a** Chondrite-normalized REE diagrams: **b** primitive mantle-normalized trace element distribution spiderdiagrams. The normalization values are from Sun and McDonough (1989)

Table 4 Sr-Nd isotopic compositions for the granite and diorite rocks in this study

Samples	Age (Ma)	Sm (ppm)	Nd (ppm)	$^{147}Sm/^{144}Nd$	$^{143}Nd/^{144}Nd$	2σ	$(^{143}Nd/^{144}Nd)_i$	ε_{Nd} (t)	Rb (ppm)	Sr (ppm)	$^{87}Rb/^{86}Sr$	$^{87}Sr/^{86}Sr$	2σ	$(^{87}Sr/^{86}Sr)_i$
17A-44-1	238.8	27.9	209	0.1002	0.512022	7	0.511865	− 9.1	83.4	6730	0.3768	0.708525	10	0.707245
17A-44-2		20.1	65.8	0.1507	0.512044	8	0.511809	− 10.2	78.1	6340	0.8290	0.708994	9	0.706178
17A-44-3		51.8	352	0.1490	0.511997	8	0.511764	− 11.1	172	4620	0.6023	0.709846	11	0.707800
17A-44-4		60.7	464	0.0965	0.511999	6	0.511848	− 9.4	233	4010	0.2994	0.709999	12	0.708982
17A-44-6		21.3	66.2	0.1537	0.511997	6	0.511757	− 11.2	81.4	6432	0.3387	0.708395	10	0.707245
17A-44-8		61.2	471	0.1491	0.511986	7	0.511753	− 11.3	242	3935	0.3515	0.708438	9	0.707244
17A-44-10		62.3	484	0.1319	0.511964	8	0.511758	− 11.2	245	4128	0.2788	0.709938	12	0.708991
17A-45-1	238	4.10	33.2	0.1245	0.511989	7	0.511795	− 10.5	158	532	0.2469	0.711525	8	0.710689
17A-45-2		2.05	12.5	0.1405	0.512085	7	0.511866	− 9.1	158	398	0.3372	0.711813	10	0.710672
17A-45-4		0.33	2.19	0.1384	0.512084	6	0.511869	− 9.0	167	331	0.3908	0.711831	9	0.710508
17A-45-5		15.8	85.7	0.1282	0.512079	6	0.511880	− 8.8	198	696	0.3372	0.712572	12	0.711431
17A-45-6		15.6	85.4	0.1274	0.512065	7	0.511867	− 9.1	194	682	0.4979	0.713108	8	0.71142245
17A-45-9		4.13	33.1	0.1305	0.512057	6	0.511854	− 9.3	156	535	0.5885	0.713404	10	0.71141174
17A-45-12		2.06	13.3	0.1303	0.512062	6	0.511859	− 9.2	175	413	0.6090	0.713502	9	0.71144034

Table 5 Pb isotopic compositions for the rocks in this study

Sample	Age (Ma)	U (ppm)	Pb (ppm)	Th (ppm)	$^{238}U/^{204}Pb$	$^{235}U/^{204}Pb$	$^{232}Th/^{204}Pb$	$^{206}Pb/^{204}Pb$	$^{207}Pb/^{204}Pb$	$^{208}Pb/^{204}Pb$	$(^{206}Pb/^{204}Pb)_i$	$(^{207}Pb/^{204}Pb)_i$	$(^{208}Pb/^{204}Pb)_i$
17A-44-1	238.8	2.82	45.3	8.66	3.9	0.0283	12.4	17.956	15.585	38.098	17.809	15.577	37.951
17A-44-2		2.11	47.6	5.21	2.8	0.0202	7.11	17.986	15.586	38.127	17.881	15.581	38.043
17A-44-3		7.48	67.2	54.10	7.0	0.0508	52.3	18.036	15.592	38.135	17.772	15.579	37.513
17A-44-4		10.5	97.7	77.4	6.7	0.0489	51.4	17.965	15.578	38.084	17.710	15.565	37.473
17A-44-6		2.13	48.2	5.23	2.8	0.0201	7.0	17.984	15.583	38.125	17.879	15.578	38.041
17A-44-8		10.7	98.2	77.6	6.8	0.0496	51.2	17.952	15.576	38.082	17.694	15.563	37.473
17A-44-10		11.2	98.4	78.1	7.1	0.0518	51.4	17.875	15.583	38.126	17.606	15.569	37.517
17A-45-1	238	3.44	37.7	17.2	5.6	0.0408	29.1	17.404	15.480	37.442	17.192	15.469	37.098
17A-45-2		2.75	37.6	10.5	4.5	0.0329	17.9	17.629	15.515	37.687	17.458	15.506	37.475
17A-45-4		2.80	32.9	10.4	5.3	0.0386	20.5	17.955	15.568	37.936	17.755	15.558	37.693
17A-45-5		14.0	34.0	76.2	25.5	0.1848	143	17.987	15.568	37.054	17.029	15.519	35.357
17A-45-6		13.8	33.7	75.8	25.3	0.1837	144	17.693	15.531	37.334	16.741	15.482	35.632
17A-45-9		3.42	37.5	17.4	5.7	0.0414	30.0	17.921	15.564	37.939	17.706	15.553	37.584
17A-45-12		2.76	37.6	10.6	4.6	0.0330	18.1	17.633	15.517	37.685	17.444	15.507	37.449

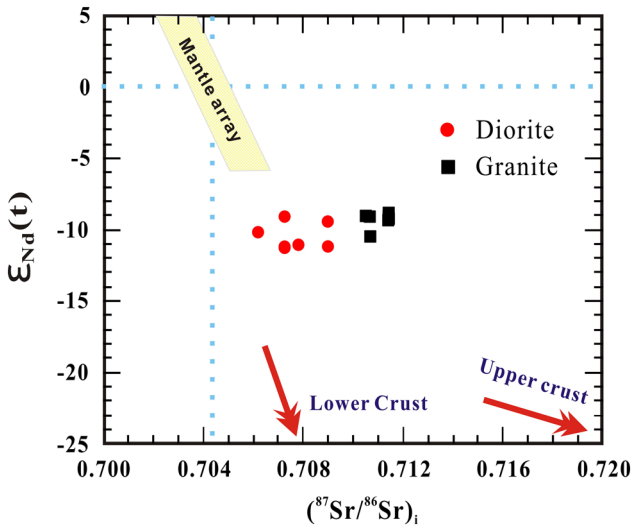

Fig. 7 Initial $^{87}Sr/^{86}Sr$ versus ε_{Nd} (t) diagram for the rocks studied from the Xinjiang Uygur Autonomous Region of South Altyn, China

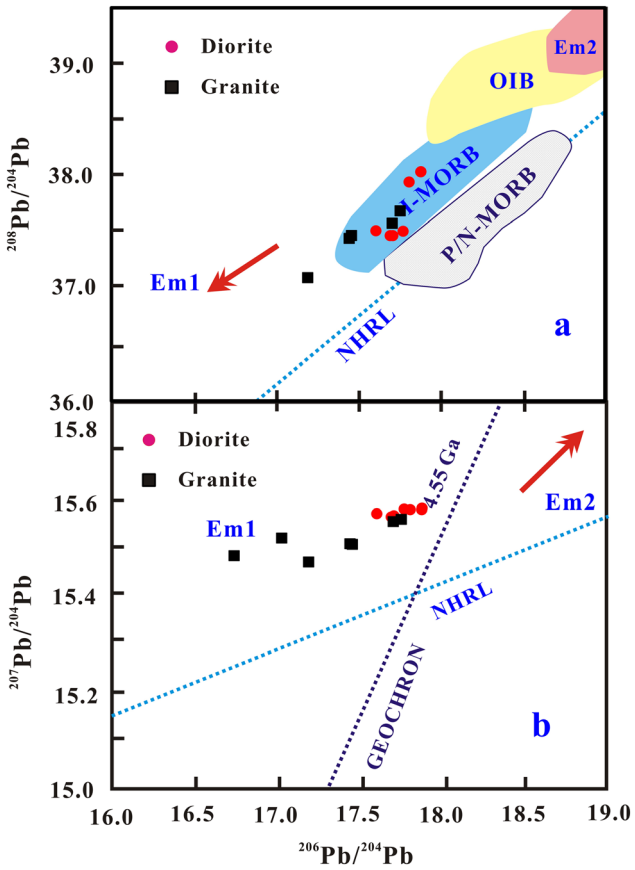

Fig. 8 $^{208}Pb/^{204}Pb$ (**a**) and $^{207}Pb/^{204}Pb$ (**b**) versus $^{206}Pb/^{204}Pb$ diagrams for the rocks studied from the Xinjiang Uygur Autonomous Region, China. Fields for I-MORB (Indian MORB) and P&N-MORB (Pacific and North Atlantic MORB), OIB, NHRL and 4.55 Ga geochron are after Barry and Kent (1998), and Hart (1984), respectively

5.3 Origins

There are clear negative correlations between MgO, TiO_2, Fe_2O_3 and SiO_2 contents (Fig. 11a–c) for the Xinjiang Uygur Autonomous Region diorite and granite samples as studied, indicating that the separation and crystallization of mafic minerals (mainly amphibole and to a lesser extent biotite) accompanied their evolution (Wang 2010; Wang et al. 2010). This observation is further supported by Th enrichment and Nb–Ta depletion in the investigated intermediate-felsic igneous rocks (Fig. 6b; Wu et al. 2001). In addition, these rocks are characterized by high Rb, Ba, Th, U, K, and LREE contents (Table 2; Fig. 6a, b), high to very high Zr/Hf ratios (133–3477), low $Mg^{\#}$ values (29–46, Table 2), and depletion in Nb, Ta, Ti, and HREE (Fig. 6). Generally, the experimental petrology theory shows that the CaO/Na_2O ratio can be used to distinguish the characteristics of intermediate to felsic magmatic rocks (Kang et al. 2016a, b). The CaO/Na_2O ratio for the investigated diorite samples falls between 0.95 and 1.31, indicating that the original rock (as melted) should be clastic rock with a small proportion of mudstone. By contrast, except for samples, 17A-45-6 and 17A-45-8, the relatively high CaO/Na_2O (0.55, 0.54), the high CaO/Na_2O ratio (0.15–0.27) of the granite indicates that the original rock should be a feldspar poor and clay-rich mudstone. Moreover, the investigated Xinjiang Uygur Autonomous Region rocks have high zircon contents and determined saturation temperatures of (T = 731–909 °C), which suggests that the zircon in the parent magmas reached saturation. Such a temperature range likely represents the initial magma temperature of their parental magmas (Miller et al. 2003; Zhao 2010). Further, in the SiO_2 versus TiO_2 temperature diagrams (Fig. 12), the determined temperature of both magmas is lower than 900 °C.

The Xinjiang Uygur Autonomous Region granite samples have relatively high SiO_2 (65.67–72.96 wt %), Al_2O_3 (> 14.53 wt %), K_2O (> 5.03 wt %), and $K_2O + Na_2O$ (9.46–11.81 wt %) values (Table 2). By contrast, the studied diorite from this area is characterized by relatively low SiO_2, K_2O, and $K_2O + Na_2O$ values (Table 2). The high CaO/Na_2O ratio (0.95–1.31) indicates that the crust involved in magma generation should be at less than 30 km depth or crustal thickness (Zhang et al. 2006). The continued thickening of the Earth's crust in this region of Asia resulted in lithospheric extension and collapse, leading to large-scale upwelling of hot asthenosphere materials. This rise of the asthenosphere can induce crustal melting. The resulting parent melts, after a certain degree of fractional crystallization, may buoyantly rise to be emplaced along with extensional fractures, to coalesce forming a large number of intermediate-felsic intrusions of Mesozoic age in the Xinjiang Uygur Autonomous Region. Thus, we

Table 6 Zircon Hf isotopic compositions of the rocks in this study

17A-44	$^{176}Yb/^{177}Hf$	2σ	$^{176}Lu/^{177}Hf$	2σ	$^{176}Hf/^{177}Hf$	2σ	$\varepsilon_{Hf}(t)$	T_{DM1} (Ma)	T_{DM2} (Ma)	$f_{Lu/Hf}$
1	0.018363	0.000118	0.000643	0.000001	0.282335	0.000016	− 10.3	1283	1917	− 0.98
2	0.018107	0.000084	0.000615	0.000001	0.282331	0.000015	− 10.5	1289	1927	− 0.98
3	0.038718	0.000675	0.001338	0.000027	0.282336	0.000017	− 10.4	1307	1923	− 0.96
4	0.050188	0.000104	0.001708	0.000010	0.282386	0.000018	− 8.7	1248	1814	− 0.95
5	0.003592	0.000091	0.000149	0.000002	0.282338	0.000015	− 10.1	1263	1906	− 1.00
6	0.015757	0.000174	0.000546	0.000007	0.282325	0.000015	− 10.7	1295	1939	− 0.98
7	0.037172	0.000056	0.001285	0.000006	0.282334	0.000017	− 10.5	1308	1927	− 0.96
8	0.018353	0.000162	0.000647	0.000008	0.282342	0.000016	− 10.1	1275	1903	− 0.98
9	0.030394	0.000431	0.001091	0.000020	0.282347	0.000017	− 10.0	1282	1895	− 0.97
10	0.014035	0.000238	0.000526	0.000010	0.282334	0.000022	− 10.4	1282	1920	− 0.98
11	0.018916	0.000070	0.000647	0.000001	0.282334	0.000014	− 10.4	1285	1920	− 0.98
12	0.015036	0.000073	0.000533	0.000001	0.282328	0.000016	− 10.6	1290	1932	− 0.98
13	0.021726	0.000083	0.000763	0.000001	0.282331	0.000016	− 10.5	1293	1928	− 0.98
14	0.009523	0.000114	0.000353	0.000004	0.282333	0.000014	− 10.3	1277	1919	− 0.99
15	0.021109	0.000572	0.000707	0.000015	0.282309	0.000017	− 11.2	1322	1976	− 0.98
16	0.039045	0.000520	0.001317	0.000022	0.282316	0.000015	− 11.1	1334	1966	− 0.96
17	0.018535	0.000768	0.000635	0.000019	0.282332	0.000020	− 10.4	1287	1923	− 0.98
18	0.020696	0.000292	0.000771	0.000015	0.282328	0.000022	− 10.6	1297	1934	− 0.98
19	0.009956	0.000182	0.000360	0.000004	0.282310	0.000018	− 11.2	1309	1972	− 0.99
20	0.013742	0.000061	0.000445	0.000002	0.282322	0.000016	− 10.8	1296	1946	− 0.99
21	0.012525	0.000066	0.000439	0.000001	0.282322	0.000016	− 10.7	1294	1944	− 0.99
22	0.021640	0.000088	0.000699	0.000008	0.282326	0.000015	− 10.6	1298	1938	− 0.98
23	0.014802	0.000038	0.000506	0.000001	0.282340	0.000013	− 10.1	1273	1906	− 0.98
24	0.025840	0.000232	0.000958	0.000011	0.282325	0.000016	− 10.7	1309	1944	− 0.97
25	0.016360	0.000253	0.000546	0.000005	0.282311	0.000013	− 11.1	1314	1970	− 0.98
17A-45	$^{176}Yb/^{177}Hf$	2σ	$^{176}Lu/^{177}Hf$	2σ	$^{176}Hf/^{177}Hf$	2σ	$\varepsilon_{H\ f}(t)$	T_{DM1} (Ma)	T_{DM2} (Ma)	$f_{Lu/Hf}$
1	0.009902	0.000032	0.000354	0.000003	0.282153	0.000018	− 16.7	1524	2321	− 0.99
2	0.013225	0.000287	0.000473	0.000009	0.282099	0.000015	− 18.7	1603	2440	− 0.99
3	0.010382	0.000058	0.000380	0.000002	0.282215	0.000018	− 14.5	1440	2182	− 0.99
4	0.014859	0.000260	0.000528	0.000005	0.282100	0.000017	− 18.6	1603	2438	− 0.98
5	0.011174	0.000226	0.000385	0.000006	0.282115	0.000015	− 18.1	1577	2404	− 0.99
6	0.011300	0.000269	0.000396	0.000008	0.282154	0.000016	− 16.7	1524	2318	− 0.99
7	0.015242	0.000193	0.000551	0.000009	0.282202	0.000016	− 15.0	1464	2212	− 0.98
8	0.011865	0.000045	0.000439	0.000003	0.282139	0.000020	− 17.2	1547	2352	− 0.99
9	0.008250	0.000182	0.000310	0.000008	0.282107	0.000020	− 18.4	1585	2422	− 0.99
10	0.007654	0.000149	0.000271	0.000004	0.282183	0.000017	− 15.7	1480	2253	− 0.99
11	0.008237	0.000046	0.000294	0.000002	0.282109	0.000016	− 18.3	1583	2418	− 0.99
12	0.006041	0.000285	0.000238	0.000008	0.282182	0.000015	− 15.7	1480	2254	− 0.99
13	0.011006	0.000314	0.000387	0.000008	0.282174	0.000016	− 16.0	1497	2274	− 0.99
14	0.013366	0.000414	0.000476	0.000016	0.282141	0.000017	− 17.2	1546	2348	− 0.99
15	0.013197	0.000641	0.000473	0.000021	0.282105	0.000019	− 18.5	1595	2428	− 0.99
16	0.007373	0.000150	0.000300	0.000005	0.282193	0.000017	− 15.3	1467	2230	− 0.99
17	0.009617	0.000040	0.000356	0.000002	0.282143	0.000017	− 17.1	1538	2342	− 0.99
18	0.014770	0.000298	0.000552	0.000008	0.282195	0.000021	− 15.3	1475	2229	− 0.98
19	0.010008	0.000069	0.000347	0.000001	0.282121	0.000015	− 17.9	1568	2392	− 0.99
20	0.008145	0.000407	0.000319	0.000012	0.282153	0.000018	− 16.7	1523	2321	− 0.99
21	0.011266	0.000268	0.000392	0.000009	0.282108	0.000017	− 18.3	1587	2420	− 0.99
22	0.010240	0.000380	0.000383	0.000010	0.282164	0.000013	− 16.4	1510	2296	− 0.99

Table 6 continued

17A-45	$^{176}Yb/^{177}Hf$	2σ	$^{176}Lu/^{177}Hf$	2σ	$^{176}Hf/^{177}Hf$	2σ	$\varepsilon_{H\ f}(t)$	T_{DM1} (Ma)	T_{DM2} (Ma)	$f_{Lu/Hf}$
23	0.011075	0.000538	0.000399	0.000016	0.282152	0.000014	− 16.8	1527	2322	− 0.99
24	0.011289	0.000466	0.000388	0.000017	0.282151	0.000015	− 16.8	1528	2325	− 0.99
25	0.009421	0.000328	0.000333	0.000010	0.282163	0.000016	− 16.4	1510	2297	− 0.99

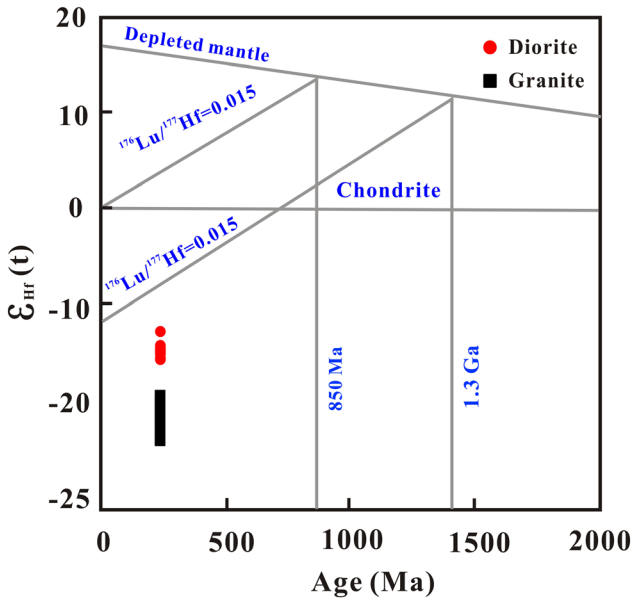

Fig. 9 Age versus ε_{Hf} (t) plot for the zircons from the rocks studied from the Xinjiang Uygur Autonomous Region, China

envisage complex tectonism resulted in the conditions necessary for the partial melting of crustal materials, providing the source magmas to the diorite and granite investigated herein.

6 Conclusions

Integrated zircon U–Pb geochronology, whole-rock geochemistry and Sr–Nd–Pb–Hf isotopic studies of a suite of intermediate-felsic igneous rocks from within the Xinjiang Uygur Autonomous Region of South Altyn, China allow us to draw the following conclusions.

1. The diorite and granite rocks from the Xinjiang Uygur Autonomous Region study area were intruded during the Triassic as evidenced in the newly determined zircon U–Pb ages, of 238.8 ± 1.1 and 238 ± 1.5 Ma.
2. All of the investigated rocks have an alkaline affinity. They are enriched in LREE, and select LILE (e.g., Rb, Ba, Sr, K), Th, U, and Pb, and depleted in HFSEs (i.e., Nb, Ta, Hf, and Ti) relative to a primitive mantle. The Xinjiang Uygur Autonomous Region granite and diorite have high initial $^{87}Sr/^{86}Sr$ ratios (0.7062–0.7114), negative ε_{Nd} (t) values (− 8.8 to − 11.3), ε_{Hf} (t) values (−8.7 to −18.7), and relatively constant Pb isotopic ratios [$(^{206}Pb/^{204}Pb)_i$ = 16.74–17.884, $(^{207}Pb/^{204}Pb)_i$ = 15.51–15.58, and $(^{208}Pb/^{204}Pb)_i$ = 35.36–38.04]. These data suggest that the magmas parental to these rock suites were generated by partial melting of the crust.
3. Based upon our findings, we suggest that the investigated Mesozoic granite and diorite rocks from the Xinjiang Uygur Autonomous Region owe their origins to crustal thickening and extensional relaxation, which promoted upwelling of asthenosphere mantle. The uplifted hot mantle caused a rise in the geothermal gradient of the overlying crust and corresponding partial melting of heterogeneous lithologies. The resulting parental magmas of intermediate and felsic composition ascended through the crust to be emplaced as granite and diorite igneous rocks in the Xinjiang Uygur Autonomous Region of South Altyn, China. Such extensional tectonics also promoted crustal thinning and possible rifting, providing important pathways for magma ascent and emplacement.

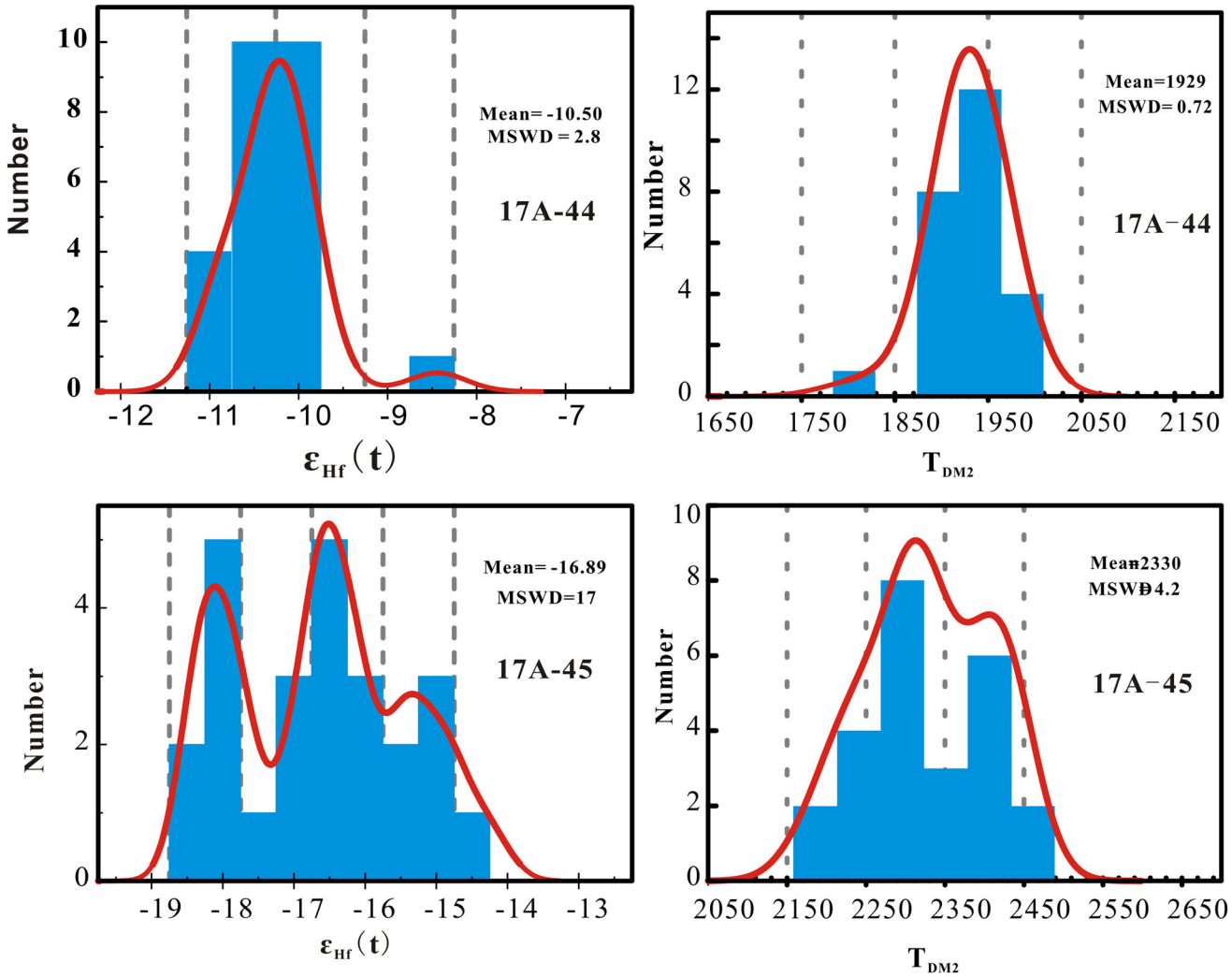

Fig. 10 Histograms of zircon ε_{Hf} (t) values and two-stage Hf model ages for the investigated granite and diorite rocks in this study

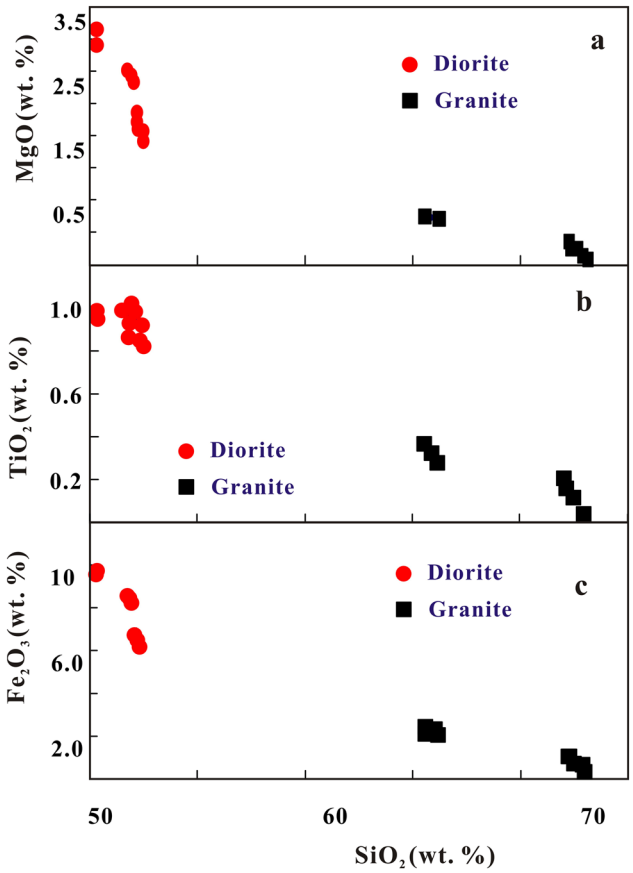

Fig. 11 SiO_2 versus MgO, TiO_2, and Fe_2O_3 plots for the rocks studied from the Xinjiang Uygur Autonomous Region, China

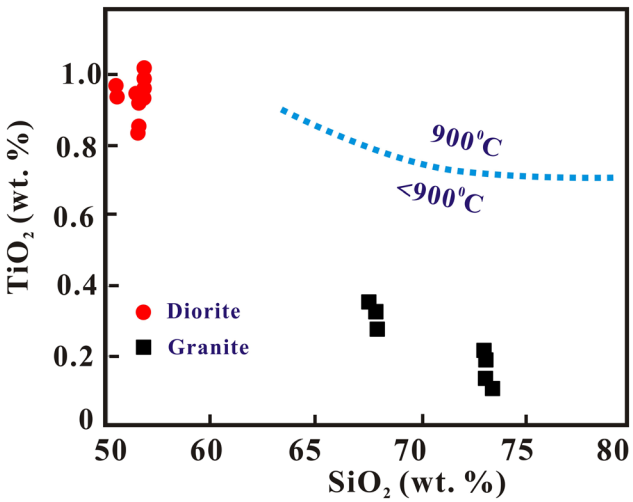

Fig. 12 The SiO_2 versus TiO_2 temperature diagram for the rocks studied from the Xinjiang Uygur Autonomous Region, China

Acknowledgments The authors would like to thank Dr. Shuqin Yang for his assistance with the XRF analyses, Prof. Liang Qi and Xiaobiao Li for their assistance during the ICP-MS analyses, the technician for assistance during the TIMS Sr–Nd–Pb isotopic analyses, and Prof. Xiaoming Liu for his assistance with the LA-ICP-MS U–Pb dating, upon which data this paper was written. This study was supported by the National Natural Science Foundation of China (Grant No.: 41573022).

References

Barry TL, Kent RW (1998) Cenozoic magmatism in Mongolia and the origin of central and East Asian basalts. In: Flower MFJ, Chung SL, Lo CH, Lee TY (Eds.), Mantle Dynamics, and Plate Interactions in East Asia. American Geophysical Union-Geodynamics Series 27: 347–364

Cao YT, Liu L, Wang C, Chen DL, Zhang AD (2009) P-T path of early Paleozoic pelitic high-pressure granulite from Danshuiguan area in Altyn Tagh. Acta Petrol Sin 25:2260–2270 **(in Chinese with English abstract)**

Cao YT, Liu L, Wang C, Yang WQ, Zhu XH (2010) Geochemical, zircon U-Pb dating, and Hf isotope compositions study for Tatelekebulake granite in south Altyn Tagh. Acta Petrol Sin 26:3259–3271 **(in Chinese with English abstract)**

Chappell BW, White AJR (1974) Two contrasting granite types. Pac Geol 8:173–174

Che ZC, Sun Y (1996) The age of the Altyn granulite facies complex and the basement of the Tarim Basin. Rigional Geology of China 1:51–57 **(in Chinese with English abstract)**

Chen HJ (2018) Genesis of Neoproterozoic granites in Altyn and its geodynamic significance. China University of Geosciences (in Chinese with English abstract)

Chen ZC, Liu L, Liu HF, Luo JH (1995) Discovery of high pressure metamorphic argillaceous rocks in Altyn mountain area and their occurrence environment. Chin Sci Bull 40:1298–1300 **(in Chinese)**

Chen ZC, Liu L, Liu HF, Luo JH (1998) The constituents of the Altyn Fault system and genetic characteristics of related Meso-Cenozoic petroleum-bearing basin. Region Geol China 7:375–384 **(in Chinese with English abstract)**

Cui JW, Tang ZM, Deng JF (1999) Altyn fault system. Geological Publishing House, Beijing **(in Chinese with English abstract)**

Cui JW, Zhang XW, Li PW (2002) The altyn fault: its geometry, nature and mode of growth. Acta Geoscientia Sinica 23:509–516 **(in Chinese with English abstract)**

Fan Y, Liu S, Feng C, Coulson IM, Liu L, Wang C (2019) U-Pb geochronology, whole-rock geochemical and Sr-Nd-Pb-Hf isotopic compositions: constraints on the origin and geodynamic setting of Neoproteozoic granitoids from the South Altyn Terrane, Tibetan Plateau. Geochem J 53:379–406

Goolaerts A, Mattielli N, de Jong J, Weis D, Scoates JS (2004) Hf and Lu isotopic reference values for the zircon standard 91500 by MC-ICP-MS. Chem Geol 206:1–9

Guo ZJ, Zhang ZC, Zhang C, Liu C, Zhang Y, Wang J, Chen WM (2008) Lateral growth of the Altyn Tagh strike-slip Fault at the north margin of the Qinghai-Tibet Plateau: late Cenozoic strike-slip Faults and the crustal stability in the Beishan area, Gansu, China. Geol Bull China 27:1678–1686 **(in Chinese with English abstract)**

Harris AC, Allen CM, Bryan SE, Compbell IH, Holcombe RJ, Palin JM (2004) ELA-ICP-MS U-Pb zircon geochronology of regional volcanism hosting the Bajo de la Alumbrera Cu-Au deposits: implications for porphyry-related mineralization. Miner Deposita 39:46–67

Hart SR (1984) A large-scale isotope anomaly in the Southern Hemisphere mantle. Nature 309:753–757

Huang LG, Zhong JH, Wang HQ, Zhao MF, Chen HL, Li Y (2004) Evolution simulation of stress field in west Qaidam Basin, NW China. Petrol Explor Dev 31:75–77 **(in Chinese with English abstract)**

Iizuka T, Hirata T (2005) Improvements of precision and accuracy in in situ Hf isotope microanalysis of zircon using the laser ablation-MC-ICPMS technique. Chem Geol 220:121–137

Jahn BM, Wu FY, Chen B (2000) Granitoids of the Central Asian Orogenic Belt and continental growth in the Phanerozoic. Trans R Soc Edinbur: Earth Sci 91:181–193

Ji WB, Lin W, Faure M, Chen Y, Chu Y, Xue ZH (2016) Origin of the Late Jurassic to Early Cretaceous peraluminous granitoids in the northeastern Hunan province (middle Yangtze region), South China: geodynamic implications for the Paleo-Pacific subduction. J Asian Earth Sci 141:174–193

Kang L, Liu L, Cao YT, Wang C, Yang WQ, Liang S (2013) Geochemistry, zircon U-Pb age and its geological significance of the gneissic granite from the eastern segment of the Tatelekebulake composite granite in the south Altyn Tagh. Acta Petrol Sin 29:3039–3048 **(in Chinese with English abstract)**

Kang L, Xiao PX, Gao XF, Xi RG, Yang ZC (2016a) Chronology, geochemistry and petrogenesis of monzonitic granite and quartz diorite in Mangai area: its inspiration to early Paleozoic tectonic-magmatic evolution of the southern Altyn Tagh. Acta Petrol Sin 32:1731–1748 **(in Chinese with English abstract)**

Kang L, Xiao PX, Gao XF, Xi RG, Yang ZC (2016b) Early Paleozoic magmatism and collision orogenic process of the South Altyn. Acta Geol Sin 90:2527–2550 **(in Chinese with English abstract)**

Le Maitre RW (2002) Igneous rocks: a classification and glossary of terms, 2nd edn. Cambridge University Press, Cambridge, p 236

Li XM, Ma ZP, Sun JM, Xue XY, Lei YX, Wang LS, Duan XX (2009) Characteristics and age study about the Yuemakeqi mafic-ultramafic rock in the southern Altyn Fault. Acta Petrol Sin 25:862–872 **(in Chinese with English abstract)**

Li Q, Zeng ZC, Chen N, Zhao JL, Zhang RY, Yi PF, Gao HF, Bi ZJ (2015) Zircon U-Pb ages, geochemical characteristics and tectonic implications of neoproterozoic gailike gneiss in the South Altyn Tagh. Geoscience 29:1271–1283 **(in Chinese with English abstract)**

Li Q, Qing JG, Ma DC, Yang FQ, Zhang ZL, Yang CD (2020) Geochronology, geochemistry and significance of the gneissic granodiorite from shayikenbulake Be deposit in Altay, Xinjiang. Acta Petrol Sin 36:948–966 **(in Chinese with English abstract)**

Liu L, Che ZC, Luo JH, Wang Y, Gao ZJ (1996) Determination of eclogites in the western part of Altyn Tagh and its geological significance. Chin Sci Bull 41:1458–1488 **(in Chinese)**

Liu L, Che ZC, Luo JH, Wang Y, Gao ZJ (1997) Recognition and implication of eclogite in the western Altyn Mountains, Xinjiang. Chin Sci Bull 42:931–934 **(in Chinese)**

Liu L, Che ZC, Wang Y, Luo JH, Wang JQ, Gao ZJ (1998) Sm-Nd isochron age evidence of early paleozoic ophiolites in Mangya area, Altyn. Chin Sci Bull 43:880–883 **(in Chinese)**

Liu L, Sun Y, Xiao PX, Che ZC, Luo JH, Chen DL, Wang Y, Zhang AD, Chen L, Wang YH (2002) Discovery of ultrahighpressure magnesite-bearing garnet lherzolite (> 3.8GPa) in the Altyn Tagh, Northwest China. Chin Sci Bull 47:881–886 **(in Chinese)**

Liu L, Sun Y, Luo JH, Wang Y, Chen DL, Zhang AD (2003) Ultrahigh-pressure metamorphism of granitic gneiss in the Yinggelisayi area, Altyn Monutains, NW China. Sci China (D) 47:338–346

Liu L, Sun Y, Luo JH, Wang Y, Chen DL, Zhang AD (2004) Ultrahigh pressure metamorphism of granitic gneiss in the Yinggelisayi area. Altyn Mountains, NW China. Sci China (D) 47:338–346

Liu L, Chen DL, Zhang AD, Sun Y, Wang Y, Yang JX, Luo JH (2005) Ultrahigh pressure gneissic K-feldspar garnet clinopyroxenite in the Altyn Tagh, NW China: evidence from clinopyroxene exsolution in garnet. Sci China (D) 48:1000–1010

Liu L, Zhang AD, Chen DL, Yang JX, Luo JH, Wang C (2007a) Implications based on LA-ICP-MS zircon U-Pb ages of eclogite and its country rock from Jianggalesayi area, Altyn Tagh. Earth Sci Front 14:98–107 **(in Chinese with English abstract)**

Liu L, Zhang J, Green HW II, Jin Z, Bozhilov KN (2007b) Evidence of former stishovite in metamorphosed sediments, implying subduction to > 350 km. Earth Planet Sci Lett 263:180–191

Liu L, Chen DL, Wang C, Zhang CL (2009a) New progress on geochronology of high-pressure/ultrahigh-pressure metamorphic rocks from the South Altyn Tagh, the North Qaidam and the North Qinling orogenic, NW China and their geological significance. J Northwest Univ (Nat Sci Edn) 39:472–479 **(in Chinese with English abstract)**

Liu L, Wang C, Chen DL, Zhang AD, Liou JG (2009b) Petrology and geochronology of HP-UHP rocks from the South Altyn Tagh, northwestern China. J Asian Earth Sci 35:232–244

Liu YS, Yu HF, Xin HT, Lu SN, Xiu QY (2009c) Tectonic units division and Precambrian significant geological events in Altyn Tagh Mountain, China. Geol Bull China 28:1430–1438 **(in Chinese with English abstract)**

Liu L, Wang C, Cao YT, Chen DL, Kang L, Yang WQ, Zhu XH (2012) Geochronology of multi-stage metamorphic events: constraints on episodic zircon growth from the UHP eclogite in the South Altyn, NW China. Lithos 136–139:10–26

Liu L, Kang L, Cao YT, Yang WQ (2015) Early Paleozoic granitic magmatism related to the processes from subduction to collision in South Altyn, NW China. Sci China: Earth Sci 45:1126–1137 **(in Chinese with English abstract)**

Lu SN, Yuan GB (2003) Geochronology of early Precambrian magmatic activities in Aketashitage, East Altyn Tagh. Acta Geol Sin 77:61–68 **(in Chinese with English abstract)**

Lu SN, Li HK, Zhang CL, Niu GH (2008) Geological and geochronological evidence for the Precambrian evolution of the Tarim Craton and surrounding continental fragments. Precambr Res 160:94–107

Luo JH, Lei GL, Liu L, Xiao ZY, Wei HX, Che ZC (2009) The Controlling of Altyn Structural Belt on Petroleum Geology of the Southeastern Part of the Tarim Basin, NW China. Geotectonica et Metallogenia 33:076–85 **(in Chinese with English abstract)**

Ma ZP, Li XM, Sun JM, Xue XY, Lei YX, Wang LS, Duan XX (2009) Discovery of layered mafic-ultramafic intrusion in Changshagou, Altyn Tagh, and it geological implication: a pilot study on its petrological and geochemical characteristics. Acta Petrol Sin 4:793–804 **(in Chinese with English abstract)**

Maniar PD, Piccoli PM (1989) Tectonic discrimination of granitoids. Geol Soc Am Bull 101:635–643

Middlemost EAK (1994) Naming materials in the magma/igneous rock system. Earth Sci Rev 74:193–227

Miller CF, McDowell SM, Mapes RW (2003) Hot and cold granites? Implications of zircon saturetion temperatures and preservation of inhertance. Geology 31:529–532

Ni JL, Wang JC, Lv BF, Lin YX, Xia B (2008) Structureal features of the Altyn Mountain and its fault systems during Mesozoic and Cenozoic. J Guilin Univ Technol 28:295–300 **(in Chinese with English abstract)**

Pan XF, Jiao JG, Wu CL, Gao YH, Zheng K, Gao D, Wu D, Guo WF, Chen HJ (2016) Zircon U-Pb dating and Hf isotope characteristics of the Aketishan granite in the southern margin of Altyn

and their tectonic implications. Acta Geoligca Sinica 93:633–646 **(in Chinese with English abstract)**

Qi L, Hu J, Gregoire DC (2000) Determination of trace elements in granites by inductively coupled plasma mass spectrometry. Talanta 51:507–513

Qin XF, Li J, Lu JP, Xu H, Hu GA, Zhou FS, Li Q (2006) Tectonic evolution of the western segment of the Altyn Tagh collisional orogen, Northwest China. Geol Bull China 25:104–112 **(in Chinese with English abstract)**

Song SG, Su L, Li XH, Niu YL, Zhang LF (2012) Grenville-age orogenesis in the Qaidam-Qilian block: the link between South China and Tarim. Precambr Res 220–221:9–22

Sun SS, McDonough WF (1989) Chemical and isotopic systematics of oceanic basalts: implications for mantle composition and processes. In: Saunders AD, Norry MJ (eds) Magmatismin the ocean basins, vol 42. Geological Society Special Publication, London, pp 313–345

Sun JM, Ma ZP, Tang Z, Li XM (2012) LA-ICP-MS Zircon dating of the Yumuquan magma mixing granite in the southern Altyn Tagh and its tectonic significance. Acta Geol Sin 2:247–257 **(in Chinese with English abstract)**

Suo ST, Zhong ZQ, Zhou HW, You ZD (2004) On the relationship between the two UHP metamorphic belts in the central orognic belt, China. Acta Gelogica Sinica 78:155–165 **(in Chinese with English abstract)**

Taylor SR, McClennan SM (1985) The cotinental crust: its composition and evolution. Blackwell Scientific Publications, Oxford, pp 1–132

Tian LP (2009) Late Paleaozoie Granitie Rocks and mineralization of the south margin of the Altyn Mountains. Ph.D. thesis of Lanzhou University **(in Chinese with English)**

Wang E (1997) Displacement and timing along the northern strand of the Altyn Tagh fault zone, Northern Tibet. Earth Planet Sci Lett 150:55–64

Wang T (2010) Genesis and Geodynamic Significance of Mesozoic alkaline rocks in Sulu orogenic belt. Ph.D thesis of Institute of Geochemistry, Chinese Academy of Sciences **(in Chinese with English abstract)**

Wang Y, Liu L, Che ZC, Chen DL, Luo JH (1999) Geochemical characteristics of early Paleozoic ophiolite in Mangnai area, Altyn Mountains. Geol Rev 45:1010–1014 **(in Chinese with English abstract)**

Wang C, Liu L, Che ZC, Chen DL, Zhang AD, Luo JH (2006) U-Pb Geochronology and Tectonic Setting of the Granitic Gneiss in Jianggaleisayi Eclogite Belt, the Southern Edge of Altyn Tagh. Geol J China Univ 12:74–82 **(in Chinese with English abstract)**

Wang C, Liu L, Zhang AD, Yang WQ, Cao YT (2008) Geochemistry and petrography of early Paleozoic Yusupuleke Tagh rapakivitetured granite complex, south Altyn: a example for magma mixing. Acta Petrol Sin 24:2809–2819 **(in Chinese with English abstract)**

Wang T, Liu S, Hu RZ, Feng CX, Qi YQ, Feng GY, Yang YH (2010) Petrogenesis of alkaline rocks in the Sulu Orogen evidence from elemental geochemistry. Acta Miner Sinica 30:194–206 **(in Chinese with English abstract)**

Wang C, Liu L, Chen DL, Cao YT (2011) Petrology, geochemistry, geochronology and metamorphic evolution of garnet peridotites from South Altyn UHP terrane, NW China: records related to crustal slab subduction and exhumation history. In: Dobrzhinetskaya L, Cuthbert S, Faryad W, Wallis S (eds) Uhpm: 25 years after discovery of coesite and diamond. Elsevier, New York, pp 541–577

Wang LS, Yang PF, Duan XX, Long XP, Sun JM (2019) Isotopic age and genesis of plagiogranite from Qingshuiquan area in the middle of South Altyn Tagh. Acta Petrol Sin 32:759–774 **(in Chinese with English abstract)**

White AJR, Chappell BW (1983) Granitoid types and their distribution in the Lachlan Fold Belt, southeastern Australia. In: Roddick JA (ed) Circum-pacific plutonic terranes, vol 159. Geological Society of America, New York, pp 21–34

Woodhead J, Hergt J, Shelley M, Eggins S, Kemp R (2004) Zircon Hf-isotope analysis with an excimer laser, depth profiling, ablation of complex geometries, and concomitant age estimation. Chem Geol 209:121–135

Wu FY, Wilde S, Sun DY (2001) Zircon SHRIMP U-Pb ages of gnessic granites in Jiamusi massif, northeastern China. Acta Petrol Sin 17:443–452 **(in Chinese with English abstract)**

Wu RX, Zheng YF, Wu YB, Zhao ZF, Zhang SB, Liu XM, Wu FY (2006) Reworking of juvenile crust: element and isotope evidence from Neoproterozoic granodiorite in South China. Precambr Res 146:179–212

Wu FY, Li XH, Yang JH, Zheng YF (2007) Discussions on the petrogenesis of granites. Acta Petrol Sin 23:1217–1238 **(in Chinese with English abstract)**

Wu L, Gong QL, Qin SH (2013) When did Cenozoic left-slip along the Altyn Tagh Fault initiate? A comprehensive approach. Acta Petrol Sin 29:2837–2850 **(in Chinese with English abstract)**

Wu CL, Gao YH, Lei M, Qin HP, Liu CH, Li MZ, Frost BR, Wooden JL (2014) Zircon SHRIMP U-Pb dating, Lu-Hf isotopic characteristics and petrogenesis of the Palaeozoic granites in Manya area, southern Altyn, NW China. Acta Petrol Sin 30:2297–2323 **(in Chinese with English abstract)**

Wu CL, Lei M, Zhang X, Chen HJ, Wu J, Li TX (2016) Petrogenesis and zircon Lu-Hf isotopic characteristics of the granites from the southern Altyn area, Northwest China. Geol China 43:1853–1883 **(in Chinese with English abstract)**

Wu CL, Chen HJ, Wu D, Ernst WG (2018) Paleozoic granitic magmatism and tectonic evolution of the South Altyn block, NW China: constraints from zircon U-Pb dating and Lu-Hf isotope geochemistry. J Asian Earth Sci 160:168–199

Xiao QH, Qiu RZ, Deng JF, Li QD, Mo XX, Huang DW, Lu XX, Wang T, Wu FY, Xie CF (2005) Granitoids and continental crustal growth model in China. Geol China 32:343–352 **(in Chinese with English abstract)**

Xu ZQ, Yang JS, Zhang JX, Jian M, Li HB, Cui JW (1999) A comparison between the tectonic units on the two sides of the Altyn sinistral strip-slip Faults and the mechanism of lithospheric shearing. Acta Geol Sin 73:193–205 **(in Chinese with English abstract)**

Xu P, Wu FY, Xie LW, Yang YH (2004) Hf isotopic compositions of the standard zircons for U-Pb dating. Chin Sci Bull 49:1642–1648 **(in Chinese)**

Yang WQ, Liu L, Yu HB, Jiao PX, Cao YT (2012) Geochemistry, geochronology and zircon Hf isotopes of the Dimunalike granite in South Altyn Tagn and its geological significance. Acta Petrol Sin 28:4139–4150 **(in Chinese with English abstract)**

Zhang JX, Meng FC (2005) Sapphirine-bearing high pressure mafic granulite and its implications in the south Altyn Tagh. Chin Sci Bull 50:265–269 **(in Chinese)**

Zhang JX, Zhang ZM, Xu ZQ (1999) The ages of U-Pb and Sm-Nd for eclogite from the western segment of Altyn Tagh tectonic belt: evidence for existence of Caledonian orogenic root. Chin Sci Bull 44:1109–1112 **(in Chinese)**

Zhang JX, Xu ZQ, Yang JS, Zhang ZM, Cui JW (2001a) Petrology, Geochemistry and Geochronology of Eclogites from the Western Segment of the Altum Tectonic Belt northwestern China. Acta Geol Sin 75:186–197 **(in Chinese with English abstract)**

Zhang JX, Xu ZQ, Yang JS, Zhang ZM, Gui JW (2001b) Petrology and geochronology of eclogite from the western segment of the Altyn Tagh, north-western China. Lithos 56:187–206

Zhang JX, Xu ZQ, Yang JS, Zhang ZM, Gui JW (2001c) Petrology geochemistry and geochronology of eclogites from the western

segment of the Altum tectonic belt northwestern China. Acta Petrol Sin 75:186–197 **(in Chinese with English abstract)**

Zhang JX, Yang JS, Xu ZQ, Meng FC, Li HB, Shi RD (2002a) Evidence for UHP metamorphism of eclogites from the Altyn Mountains. Chin Sci Bull 47:751–755 **(in Chinese)**

Zhang JX, Yang JS, Xu ZQ, Meng FC, Song SG (2002b) Evidence for UHP metamorphism in Altyn eclogite. Chin Sci Bull 47:231–234 **(in Chinese)**

Zhang AD, Liu L, Sun Y, Chen DL, Wang Y, Luo JH (2004) SHRIMP U-Pb zircon ages for the UHP metamorphosed granitoid gneiss in Altyn Tagh and their geological significance. Chin Sci Bull 49:2527–2532 **(in Chinese)**

Zhang JX, Meng FC, Yang JS (2005) A new HP/LT metamorphic terrane in the northern Altyn Tagh, western China. Int Geol Rev 47:371–386

Zhang Q, Wang Y, Li CD, Wang YL, Jin WJ, Jia XQ (2006) Grenite classification on the basin of Sr and Yb contents and its implications. Acta Petrol Sin 22:2249–2269 **(in Chinese with English abstract)**

Zhang JX, Meng FC, Mattinson CG (2007) Progress, Controversies and Challenge of Studies on South Altyn Tagh-North Qaidam HP/UHP Metamorphic Belt. Geol J China Univ 13:526–545 **(in Chinese with English abstract)**

Zhao ZH (2010) Trace element geochemistry of accessory minerals and its applications in petrogenesis and metallogenesis. Earth Sci Front 17:267–286 **(in Chinese with English abstract)**

Zhao KD, Jiang SY, Zhu JC, Li L, Dai BZ, Jiang YH, Ling HF (2010) Hf isotopic composition of zircons from the Huashan-Guposhan intrusive complex and their mafic enclaves in northeastern Guangxi: implication for petrogenesis. Chin Sci Bull 55:509–519

Zhao KD, Jiang SY, Yang SY, Dai BZ, Lu JJ (2012) Mineral chemistry, trace elements and Sr-Nd-Hf isotope geochemistry and petrogenesis of Cailing and Furong granites and mafic enclaves from the Qitianling batholith in the Shi-Hang zone, South China. Gondwana Res 22:310–324

Zhao JL, Zeng ZC, Chen N, Li Q, Zhang RY, Wang X, Du B, Yuan Z (2018) Geochemical characteristics and geological significance of Binggounan Formation meta-volcanic rocks on the northern side of Yusupualeketage at the southern edge of the Altyn Mounatins. Geol Bull China 37:655–668 **(in Chinese with English abstract)**

Zheng YF, Zhang SB, Zhao ZF, Wu YB, Li XH, Li ZX, Wu FY (2007) Contrasting zircon Hf and O isotopes in the two episodes of Neoproterozoic granitoids in South China: implications for growth and reworking of continental crust. Lithos 96:127–150